Joint Estimation of Velocity, Angle-of-Arrival and Range (JEVAR) Using a Conjugate Pair of Zadoff-Chu Sequences

Zhiyu Yang, *Student Member, IEEE*, Rui Wang, *Student Member, IEEE*, Yi Jiang, *Member, IEEE*, and Jian Li, *Fellow, IEEE*

***Abstract*—This paper studies the joint estimation of velocity, AOA, and range (JEVAR) of a target in a multipath environment, which has gain renewed interest with the advent of 5G Internet of Things (IoT) technologies, owing to the numerous emerging localization-related applications. To solve the JEVAR problem, we propose a novel scheme, wherein the target transmits a pair of conjugate Zadoff-Chu (ZC) sequences and the multi-antenna receiver conducts maximum likelihood (ML) estimation. The proposed scheme is computationally efficient: it uses alternating projection (AP) to reduce the high-dimensional problem due to the multipaths to multiple lower-dimensional ones per path; it uses a conjugate pair of ZC sequences to decouple the joint estimation of the frequency and time offsets of each path into two separate estimates. The proposed scheme is highly versatile: it can resolve the multipaths with super resolution in both spatial and temporal domain; it can measure the velocity of the target via estimating the frequency offsets of the line-of-sight (LOS) signal and its multipath reflections. The simulations verify the effectiveness of the proposed scheme by showing that its performance can approach the Cramer-Rao bound (CRB).**

***Index Terms*—Angle-of-arrival, velocity, range, Zadoff-Chu sequence, maximum likelihood estimation, Cramer-Rao Bound.**

I. Introduction

THE estimation of velocity (via estimating Doppler frequency offset), angle-of-arrival (AOA), and range (via estimating time delay) of a target, is a classic radar signal processing problem [1], [2]. In recent years, this problem has gained great interest outside of the radar community, owing to the numerous localization-related applications emerging with the advent of 5G Internet of Things (IoT) technologies [3], [4], including autonomous driving [5]–[7] and indoor localization [8].

The traditional methods estimate time delay through cross correlation [9], whose performance is limited by the bandwidth. Although using interpolation [10] and matched filtering [11] can improve the resolution, they cannot resolve closely spaced multipaths. The ultra-wideband (UWB) can be used to achieve high-precision ranging [12] at a hefty hardware cost.

Given a multi-antenna receiver, the problem of joint estimation of AOA and time delay (JADE) was proposed in [13]. Two types of the JADE methods have been proposed: the subspace-based and the maximum likelihood (ML)-based. The former, such as the MUSIC [14]–[16] and the ESPRIT [17]–[19], have low computational complexity traded for suboptimal performance; the latter [20]–[23] can achieve higher resolution at the expense of higher computational complexity.

The joint estimation of velocity, AOA, and range, which we term as the JEVAR problem, was originally proposed for wireless channel estimation in [24] and was later studied for the global navigation satellite systems (GNSS) in [25]. The JEVAR problem also arises from various IoT applications, such as autonomous driving and indoor localization/navigation, as the estimates of the velocities, angles, and ranges of a source in the multipath environment can be combined for high-precision localization. In a dense urban or indoor environment, however, the JEVAR problem, and even the JADE, is challenging due to the multipath interferences.

In [24]–[26], the space-alternating generalized expectation-maximization (SAGE) method is utilized to transform the high-dimensional parameter optimization problem to multiple lower-dimensional ones. But even for the single-path LOS case, the JEVAR is a challenging three-dimensional searching problem, especially when the uncertainty ranges of the time delay and frequency offset are large. As a relevant work, paper [27] discusses a multi-source JEVAR problem in the line-of-sight (LOS) case.

In [28], the authors propose an interesting technique to drastically simplify the joint estimation of the time delay and frequency offset by introducing a conjugate pair of Zadoff-Chu (ZC) sequences. By exploiting the time delay-frequency offset ambiguity of the ZC sequences, one can reduce the two-dimensional problem to two single-dimensional ones. But the algorithm in [28] is designed for preamble acquisition and

Manuscript received January 21, 2021; revised July 4, 2021 and October 16, 2021; accepted October 19, 2021. Date of publication October 27, 2021; date of current version November 10, 2021. The associate editor coordinating the review of this manuscript and approving it for publication was Dr. Bo Tang. This work was supported in part by the National Natural Science Foundation of China under Grant 61771005. This work was presented in part at the IEEE Global Communications Conference 2021 in Madrid, Spain. *(Corresponding author: Yi Jiang.)*

Zhiyu Yang, Rui Wang, and Yi Jiang are with the Shanghai Institute for Advanced Communication and Data Science, Key Laboratory for Information Science of Electromagnetic Waves, Department of Communication Science and Engineering, Fudan University, Shanghai 200433, China (e-mail: 19210720067@fudan.edu.cn; 18110720020@fudan.edu.cn; yijiang@fudan.edu.cn).

Jian Li is with the Department of Electrical and Computer Engineering, University of Florida, Gainesville, FL 32611 USA (e-mail: li@dsp.ufl.edu).

Digital Object Identifier 10.1109/TSP.2021.3122907

channel estimation and hence cannot achieve super-resolution estimation of the time delays.

This paper studies the JEVAR problem similar to that in [24], [25], but by borrowing the idea of using conjugate ZC sequences [28], we propose a novel and more efficient solution, which has the target transmit a pair of conjugate ZC sequences and has the multi-antenna receiver conduct ML estimation. We use the alternating projection (AP) method [29] to transform the multipath problem into multiple decoupled single-path problems. For the single-path parameters estimation, the ML estimation consists of two steps: the first step is a fast initialization of the estimate by exploiting the ZC sequences' time delay-frequency offset ambiguity, and the second step is the refinement for super-resolution estimation by using Newton's iterative method.

The numerical simulation shows that the root mean square error (RMSE) performance of the proposed scheme can approach the Cramer-Rao bound (CRB) even in challenging scenarios with (very) closely-spaced multipaths. Even with only 20 MHz bandwidth (it is WiFi's bandwidth on the 2.4 GHz frequency band), the proposed scheme can achieve range estimation precision of centimeter-level, AOA estimation precision of $0.01°$, and velocity estimation precision of one meter per second (m/s), which makes the proposed scheme a promising technology for the localization and navigation related IoT applications.

The remainder of this paper is organized as follows. Section II establishes the signal model and formulates the JEVAR problem. Section III introduces the properties of ZC sequences and shows the benefit of using a conjugate pair of ZCs as the pilot. Section IV derives the solution to the JEVAR problem in the single-path case. Based on the single-path solution, Section V proposes to use the AP method to the multipath case. Numerical examples are given in Section VI and conclusions are made in Section VII.

Notations: $(\cdot)^T$, $(\cdot)^*$ and $(\cdot)^H$ stand for transpose, conjugate and Hermitian transpose, respectively. $\otimes$ denotes Kronecker product and $\odot$ denotes Hadamard (element-wise) product. $\mathbb{Z}$ is the set of integers, $\mathbb{R}$ is the set of real numbers, and $\mathbb{C}^{N\times K}$ is the set of $N\times K$ complex matrices. $\mathrm{diag}(\mathbf{a})$ denotes a diagonal matrix with vector $\mathbf{a}$ being its diagonal and $\mathrm{vec}(\cdot)$ denotes a vectorization operation to a matrix by stacking the columns of the matrix into a long column-vector. $|\cdot|$, $\|\cdot\|_F$ and $\|\cdot\|$ stand for absolute value, Frobenius norm, and l_2 norm, respectively. $\mathrm{Re}\{\cdot\}$ and $\mathrm{Im}\{\cdot\}$ stands for taking the real and imaginary part, respectively. $[\cdot]_{i,j}$ denotes the (i,j)th element of a matrix.

II. Signal Model and Problem Formulation

A. Signal Model

Consider an M-element uniform linear array (ULA) at the receiver, as shown in Fig. 1. The steering vector $\mathbf{a}(\theta)$ with respect to the AOA θ can be written as

$$\mathbf{a}(\theta)=[1,e^{-j\frac{2\pi d}{\lambda}\sin\theta},e^{-j\frac{4\pi d}{\lambda}\sin\theta},\ldots,e^{-j\frac{2\pi d(M-1)}{\lambda}\sin\theta}]^T, \tag{1}$$

where d is the inter-antenna spacing and λ is the carrier wavelength.

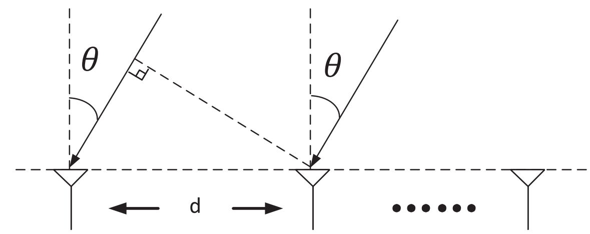

Fig. 1. Illustration of AOA with respect to ULA in a far-filed region.

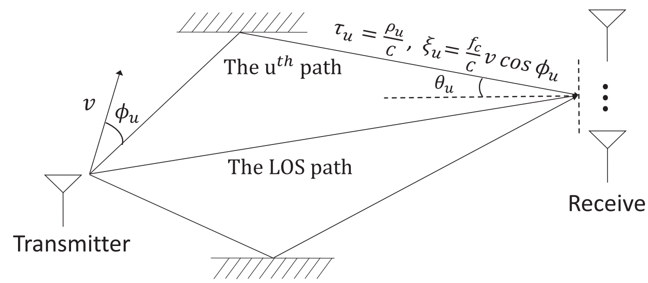

Fig. 2. Illustration of the multipath environment.

In a multipath environment, as illustrated in Fig. 2, the received signal consists of a LOS path and $U-1$ reflections of a known pilot signal $x(t)$. The Doppler frequency offset ξ is related to the velocity v of the target by

$$\xi=\frac{f_c v\cos\phi}{C}, \tag{2}$$

where C is the light speed, f_c is the carrier frequency, and ϕ is the angle between the velocity direction and that of the propagation path; the time delay τ is related to the range ρ by

$$\tau=\frac{\rho}{C}. \tag{3}$$

Superimposed by the additive white Gaussian noise $\mathbf{z}(t)$, the continuous time signal received by the antenna array is

$$\mathbf{y}(t)=\sum_{u=1}^{U}\beta_u\mathbf{a}(\theta_u)x(t-\tau_u)e^{j2\pi\xi_u t}+\mathbf{z}(t),t\in\mathbb{R}, \tag{4}$$

where θ_u, τ_u, ξ_u, and β_u denote the AOA, time delay, Doppler frequency offset, and the complex channel gain of the u^{th} path, respectively.

The sampled signal after the receiver's analog-to-digital converters (ADC) is

$$\mathbf{y}(nT_s)=\sum_{u=1}^{U}\beta_u\mathbf{a}(\theta_u)x(nT_s-\tau_u)e^{j2\pi\xi_u nT_s}+\mathbf{z}(nT_s), \quad n\in\mathbb{Z}, \tag{5}$$

where T_s is the Nyquist sampling interval. For notational simplicity, we denote $T_s=1$ without loss of generality, and thus simplify (5) to be

$$\mathbf{y}(n)=\sum_{u=1}^{U}\beta_u\mathbf{a}(\theta_u)x(n-\tau_u)e^{j2\pi\xi_u n}+\mathbf{z}(n), \tag{6}$$

where $\tau_u\in\mathbb{R}$ is not necessarily an integer.

We assume that L samples, with indices from $-L/2$ to $L/2-1$, are processed [if L is an odd number, the indices are from $-(L-1)/2$ to $(L-1)/2$]. The index range differs from the convention to cater to the proposed special design of the pilot $x(t)$, as we will see soon in Section III.

By formatting

$$\begin{aligned}
\boldsymbol{\tau} &= [\tau_1, \tau_2, \dots, \tau_U]^T \in \mathbb{R}^U,\\
\boldsymbol{\xi} &= [\xi_1, \xi_2, \dots, \xi_U]^T \in \mathbb{R}^U,\\
\boldsymbol{\theta} &= [\theta_1, \theta_2, \dots, \theta_U]^T \in \mathbb{R}^U,\\
\boldsymbol{\beta} &= [\beta_1, \beta_2, \dots, \beta_U]^T \in \mathbb{C}^U,\\
\mathbf{A}(\boldsymbol{\theta}) &= [\mathbf{a}(\theta_1), \mathbf{a}(\theta_2), \dots, \mathbf{a}(\theta_U)] \in \mathbb{C}^{M\times U},\\
\mathbf{Y} &= \left[\mathbf{y}\left(-\frac{L}{2}\right), \mathbf{y}\left(-\frac{L}{2}+1\right), \dots, \mathbf{y}\left(\frac{L}{2}-1\right)\right] \in \mathbb{C}^{M\times L},
\end{aligned}$$

and

$$\mathbf{Z} = \left[\mathbf{z}\left(-\frac{L}{2}\right), \mathbf{z}\left(-\frac{L}{2}+1\right), \dots, \mathbf{z}\left(\frac{L}{2}-1\right)\right] \in \mathbb{C}^{M\times L}, \tag{7}$$

we reformulate (6) as

$$\mathbf{Y} = \mathbf{A}(\boldsymbol{\theta})\,\mathrm{diag}(\boldsymbol{\beta})\mathbf{X}(\boldsymbol{\tau},\boldsymbol{\xi})^T + \mathbf{Z}, \tag{8}$$

where

$$\mathbf{X}(\boldsymbol{\tau},\boldsymbol{\xi}) = \left[\mathbf{x}(\tau_1)\odot\mathbf{d}(\xi_1), \dots, \mathbf{x}(\tau_U)\odot\mathbf{d}(\xi_U)\right] \in \mathbb{C}^{L\times U} \tag{9}$$

with

$$\mathbf{x}(\tau_u) = \begin{bmatrix} x(-L/2-\tau_u)\\ x(-L/2+1-\tau_u)\\ \vdots\\ x(L/2-1-\tau_u)\end{bmatrix}, \ \mathbf{d}(\xi_u) = \begin{bmatrix} e^{j2\pi\xi_u(-L/2)}\\ e^{j2\pi\xi_u(-L/2+1)}\\ \vdots\\ e^{j2\pi\xi_u(L/2-1)}\end{bmatrix}. \tag{10}$$

B. Problem Formulation

Because the elements of $\mathbf{Z}$ are of i.i.d. white Gaussian distribution, the ML estimation of the parameters $\{\boldsymbol{\beta},\boldsymbol{\tau},\boldsymbol{\xi},\boldsymbol{\theta}\}$ can be readily derived into the least square form:

$$\{\hat{\boldsymbol{\beta}},\hat{\boldsymbol{\tau}},\hat{\boldsymbol{\xi}},\hat{\boldsymbol{\theta}}\} = \arg\min_{\boldsymbol{\beta},\boldsymbol{\tau},\boldsymbol{\xi},\boldsymbol{\theta}} \left\|\mathbf{Y} - \mathbf{A}(\boldsymbol{\theta})\,\mathrm{diag}(\boldsymbol{\beta})\mathbf{X}(\boldsymbol{\tau},\boldsymbol{\xi})^T\right\|_F^2. \tag{11}$$

Since $\mathrm{vec}(\mathbf{ABC}^T) = (\mathbf{C}\otimes\mathbf{A})\mathrm{vec}(\mathbf{B})$, we have

$$\mathrm{vec}(\mathbf{A}(\boldsymbol{\theta})\,\mathrm{diag}(\boldsymbol{\beta})\mathbf{X}(\boldsymbol{\tau},\boldsymbol{\xi})^T) = \tilde{\mathbf{X}}\boldsymbol{\beta}, \tag{12}$$

where

$$\tilde{\mathbf{X}} = [\tilde{\mathbf{x}}_1, \tilde{\mathbf{x}}_2, \dots, \tilde{\mathbf{x}}_U] \in \mathbb{C}^{LM\times U}, \tag{13}$$

$$\tilde{\mathbf{x}}_u = [\mathbf{x}(\tau_u)\odot\mathbf{d}(\xi_u)]\otimes\mathbf{a}(\theta_u) \in \mathbb{C}^{LM\times 1}, u = 1, \dots, U. \tag{14}$$

Thus, (11) can be rewritten as

$$\{\hat{\boldsymbol{\beta}},\hat{\boldsymbol{\tau}},\hat{\boldsymbol{\xi}},\hat{\boldsymbol{\theta}}\} = \arg\min_{\boldsymbol{\beta},\boldsymbol{\tau},\boldsymbol{\xi},\boldsymbol{\theta}} \left\|\mathrm{vec}(\mathbf{Y}) - \tilde{\mathbf{X}}\boldsymbol{\beta}\right\|^2. \tag{15}$$

Denote $\tilde{\mathbf{y}} \triangleq \mathrm{vec}(\mathbf{Y})$, the ML estimate of $\boldsymbol{\beta}$ is

$$\hat{\boldsymbol{\beta}} = (\tilde{\mathbf{X}}^H\tilde{\mathbf{X}})^{-1}\tilde{\mathbf{X}}^H\tilde{\mathbf{y}}. \tag{16}$$

Inserting (16) into (15) yields

$$\{\hat{\boldsymbol{\tau}},\hat{\boldsymbol{\xi}},\hat{\boldsymbol{\theta}}\} = \arg\max_{\boldsymbol{\tau},\boldsymbol{\xi},\boldsymbol{\theta}} \tilde{\mathbf{y}}^H\mathcal{P}(\tilde{\mathbf{X}})\tilde{\mathbf{y}}, \tag{17}$$

where $\mathcal{P}(\tilde{\mathbf{X}}) \triangleq \tilde{\mathbf{X}}(\tilde{\mathbf{X}}^H\tilde{\mathbf{X}})^{-1}\tilde{\mathbf{X}}^H$ is the projection matrix of $\tilde{\mathbf{X}}$.

The JEVAR problem (17) is the focus of this paper, which appears difficult as it involves non-convex optimization in a $3U$-dimensional space, where the number of multipaths U can be estimated using, e.g., the Akaike's Information Criterion (AIC) or the Minimum Description Length (MDL) criterion [30]–[32], which will be discussed in Section VI. To obtain an efficient solution, we i) use a conjugate pair of ZC sequences as the pilot to decouple the estimation of the time delays and frequency offsets, and ii) use an AP method on the receiver side to obtain the optimum solution.

We first elaborate the design of the pilot and illustrate its benefit in Section III before explaining the estimation method.

III. Joint Estimation of Time Delay and Frequency Offset Based on Conjugate Pair of ZC Sequences

This section considers a subproblem of the JEVAR: to jointly estimate the time delay and frequency offset using one antenna in single-path LOS environment. We first elaborate the properties of the ZC sequences and then show how a conjugate pair of ZC sequences can be used to solve this subproblem efficiently.

A. Properties of ZC Sequence

A length-$\tilde{L}$ ZC sequence is [33]

$$s(n) = \begin{cases} e^{\frac{j\pi r n(n+1)}{\tilde{L}}} & \text{if } \tilde{L} \text{ is odd}\\ e^{\frac{j\pi r n^2}{\tilde{L}}} & \text{if } \tilde{L} \text{ is even}\end{cases}, \tag{18}$$

where the index r is a positive integer co-prime to $\tilde{L}$.

It is easy to verify that $s(n) = s(n+\tilde{L})$, i.e., the ZC is periodic. Hence we can set the index range of the ZC to be from $-\tilde{L}/2$ to $\tilde{L}/2-1$ for an even $\tilde{L}$, or from $-(\tilde{L}-1)/2$ to $(\tilde{L}-1)/2$ for an odd $\tilde{L}$.

For an even $\tilde{L}$ and an integer delay τ, we have

$$s(n-\tau) = e^{\frac{j\pi r(n-\tau)^2}{\tilde{L}}} = e^{\frac{j\pi r\tau^2}{\tilde{L}}} e^{\frac{-j2\pi r\tau n}{\tilde{L}}} s(n). \tag{19}$$

That is, an integer delay τ amounts to a frequency offset $\frac{-r}{L}\tau$; the same property also holds for an odd-length ZC. This property indicates that the time delay and frequency offset cannot be uniquely determined based on a single ZC sequence. In paper [28], the authors propose to resolve this ambiguity by using a pair of conjugate ZC sequences.

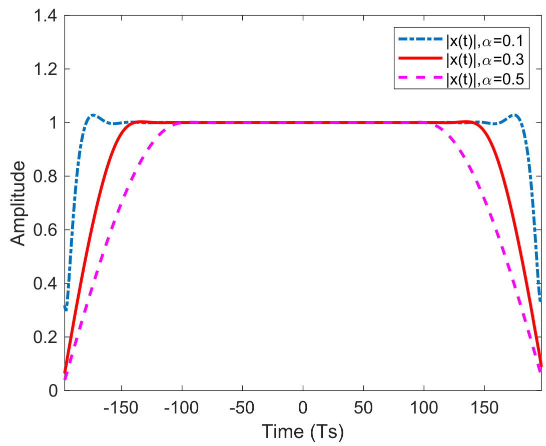

Fig. 3. The amplitude of $x(t)$ as defined in (21).

B. Pulse Shaping of Raised Cosine Filter

The time-frequency ambiguity revealed in (19) only applies to an integer τ. But to achieve super-resolution time delay estimation, we need to take into account the pulse shaping filters that is inherent to the transmitter's digital-to-analog converters (DAC) and the receiver's analog-to-digital converters (ADC).

We model the pulse shaper as the raised cosine filter with impulse response

$$p(t) = \text{sinc}(t)\frac{\cos(\pi\alpha t)}{1-(2\alpha t)^2}, \tag{20}$$

where we have assumed the Nyquist sampling interval $T_s = 1$ for notational simplicity and α is the roll-off factor. With this filtering, the ZC sequence $s(n)$ becomes a continuous-time waveform

$$x(t) = \sum_n s(n)p(t-n), \quad t \in \mathbb{R}. \tag{21}$$

The high-frequency components of the ZC sequence will be suppressed by the pulse shaping filter. As an illustrative example, Fig. 3 shows $|x(t)|$, where $x(t)$ is obtained according to (21) from a ZC sequence of length 400.[1] $|x(t)|$ is suppressed at both ends, where the sequence $s(n)$ has high frequency and thus is suppressed by the filter; the mid-part of the sequence has low frequency and thus is intact.

Indeed, the mid-part of the continuous time waveform $x(t)$ is approximately a chirp signal, i.e.,

$$x(t) \approx e^{j\pi t^2/\tilde{L}}, \quad -\frac{L}{2} \le t < \frac{L}{2}, \tag{22}$$

where $L < \tilde{L}$. The roll-off factor α will affect the choice of L as can be seen from Fig. 3. Fig. 4 shows a zoomed-in view of the difference $|x(t) - e^{j\pi t^2/\tilde{L}}|$ with $\alpha = 0.3$. In this case, the approximation (22) is quite precise for $L = 250$.

Now we have established that the lower-frequency part of the ZC sequence pulse shaped by a raised cosine filter can be approximated as a chirp $x(t) = e^{j\pi t^2/\tilde{L}}$, which also has the ambiguity between time delay and frequency offset:

[1]Here and in remainder of this paper, we only consider the ZCs with index $r = 1$.

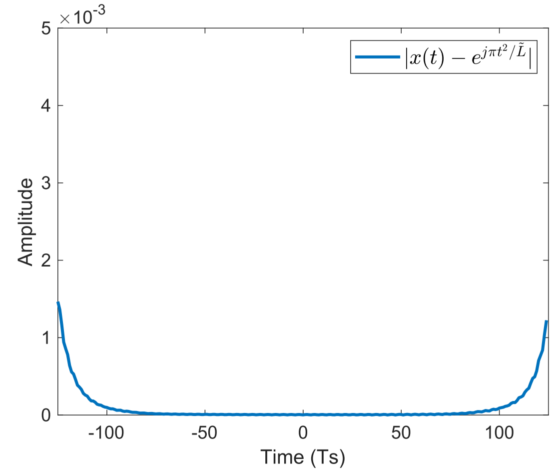

Fig. 4. The approximation (22) is good since $|x(t) - s(t)| < 1.8 \times 10^{-3}$ for $-125 \le t < 125$.

$$x(t-\tau) = e^{j\frac{\pi\tau^2}{\tilde{L}}} e^{-j\frac{2\pi\tau t}{\tilde{L}}} x(t), \tag{23}$$

where the delay τ can be a real-valued number rather than an integer in (19).

Denoting

$$\mathbf{x}(\tau) \triangleq \begin{bmatrix} x(-\frac{L}{2}-\tau) \\ x(-\frac{L}{2}+1-\tau) \\ \vdots \\ x(\frac{L}{2}-1-\tau) \end{bmatrix}, \mathbf{s} \triangleq \begin{bmatrix} s(-\frac{L}{2}) \\ s(-\frac{L}{2}+1) \\ \vdots \\ s(\frac{L}{2}-1) \end{bmatrix}, \tag{24}$$

and recognizing that $\mathbf{x}(0) = \mathbf{s}$, we can rewrite (23) in the vector form as

$$\mathbf{x}(\tau) = e^{j\frac{\pi\tau^2}{\tilde{L}}} \mathbf{s} \odot \mathbf{d}\left(-\frac{\tau}{\tilde{L}}\right), \tag{25}$$

where $\mathbf{d}(\cdot)$ is as defined in (10).

C. The Pilot Design Based on Conjugate ZC Sequences

Inspired by [28], here we also adopt the conjugate pair of ZC sequences as the pilot. But in this paper, we take the pulse shaper filtering into account and recognize that the mid-part of the continuous time waveform $x(t) = \sum_n s(n)p(t-n)$ can be approximated as a chirp signal, as illustrated in Section III. A. This observation greatly simplifies the super-resolution estimation of the time delay.

The first half pilot is

$$s(n) = e^{j\pi n^2/\tilde{L}}, n = -\frac{L}{2}, -\frac{L}{2}+1, \ldots, \frac{L}{2}-1, \tag{26}$$

and the second half is

$$s^*(n) = e^{-j\pi n^2/\tilde{L}}, n = -\frac{L}{2}, -\frac{L}{2}+1, \ldots, \frac{L}{2}-1. \tag{27}$$

For the first half pilot, we propose to append a length-$\frac{Q}{2}$ prefix and a length-$\frac{Q}{2}$ suffix as the protection interval, which

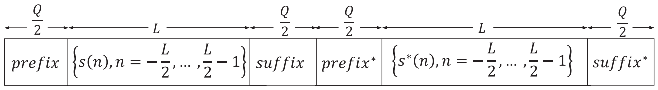

Fig. 5. The pilot sequence structure based on conjugate ZC sequences pair.

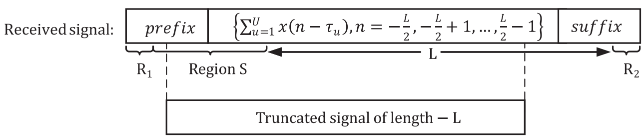

Fig. 6. The truncation of one half of the received pilot.

can be expressed as

$$prefix = e^{j\pi n^2/\tilde{L}}, n = -\frac{L+Q}{2}, \ldots, -\frac{L}{2} - 1, \tag{28}$$

and

$$suffix = e^{j\pi n^2/\tilde{L}}, n = \frac{L}{2}, \ldots, \frac{L+Q}{2} - 1. \tag{29}$$

Similarly, the second half pilot has the conjugate prefix and the conjugate suffix.

Fig. 5 depicts the structure of the conjugate ZC pilot. The prefix and the suffix can protect the pilot against not only the inter-symbol interference (ISI) but also the frequency offsets. As shown in Fig. 6, the received length-$(L+Q)$ pilot, which is smeared by the ISI of length-R_1 and the frequency offsets that amount to time offsets up to R_2, will be truncated to a length-L sequence. To make sure the whole L-length truncation does not overlap with the R_1 and R_2 regions, the truncation can start anywhere in "Region S" ("S" stands for the starting point of the truncation) of length $(L+Q-R_1-R_2)$.

As two truncations can be obtained from the pair of conjugate ZCs; the propose JEVAR algorithm will be run based on the two.

D. Joint Estimation of Time Delay and Frequency Offset

To show how using a conjugate pair of ZC sequences can simplify the estimation of time delay and frequency offset, we consider the simple case – a single-antenna receiver in a LOS single-path environment.

After being pulse shaped, the first half of the pilot sequence will be (approximately)

$$x(t) = e^{j\pi t^2/\tilde{L}}, \quad -\frac{L+Q}{2} \leq t \leq \frac{L+Q}{2} - 1, \tag{30}$$

while the second half is its conjugate.

The received signal corresponding to the first half of the pilot – with attenuation β, time delay τ, and frequency offset ξ – is

$$\begin{aligned} y(t) &= \beta x(t-\tau) e^{j2\pi\xi t} + z(t) \\ &= \beta e^{\frac{j\pi\tau^2}{\tilde{L}}} x(t) e^{j2\pi\left(\xi - \frac{\tau}{\tilde{L}}\right)t} + z(t), \end{aligned} \tag{31}$$

where the last equality holds according to (23). Here $z(t)$ is the Gaussian white noise. Interestingly, in (31) the time delay and the frequency offset are merged into one term $\xi - \frac{\tau}{\tilde{L}}$.

The receiver's ADC yields discrete samples (again, we assume the Nyquist sampling interval $T_s = 1$). The L-sample truncation as shown in Fig. 6 is

$$y_1(n) = \beta e^{\frac{j\pi\tau^2}{\tilde{L}}} s(n) e^{j2\pi\left(\xi - \frac{\tau}{\tilde{L}}\right)n} + z_1(n), n = -\frac{L}{2}, \ldots, \frac{L}{2} - 1, \tag{32}$$

where $s(n)$ is as defined in (26), and the subscript "1" stands for the "first" half of the pilot – we will use subscript "2" later for the second half of the pilot.

Although the half pilot is of length $(L+Q)$ samples, we only truncate out L samples, indexed from $-L/2$ to $L/2-1$, starting from the ISI-free region as shown in Fig. 5.

Denoting

$$\mathbf{y}_1 = [y_1(-L/2), y_1(-L/2+1), \ldots, y_1(L/2-1)]^T, \tag{33}$$

$$\mathbf{s} = [s(-L/2), s(-L/2+1), \ldots, s(L/2-1)]^T, \tag{34}$$

we have

$$\mathbf{y}_1 = \beta e^{\frac{j\pi\tau^2}{\tilde{L}}} \mathbf{s} \odot \mathbf{d}\left(\xi - \frac{\tau}{\tilde{L}}\right) + \mathbf{z}_1, \tag{35}$$

where $\mathbf{d}(\cdot)$ is as defined in (10).

Denote $\tilde{\beta} \triangleq \beta e^{\frac{j\pi\tau^2}{\tilde{L}}}$ and

$$\zeta \triangleq \xi - \frac{\tau}{\tilde{L}}. \tag{36}$$

Then (35) can be expressed as

$$\mathbf{y}_1 = \tilde{\beta}\mathbf{s} \odot \mathbf{d}(\zeta) + \mathbf{z}. \tag{37}$$

As $\mathbf{z}$'s elements are i.i.d. Gaussian, we can derive the ML estimation of $\tilde{\beta}$ and ζ as

$$\begin{aligned} \{\hat{\beta}, \hat{\zeta}\} &= \arg\min_{\tilde{\beta},\zeta} \left\| \mathbf{y}_1 - \tilde{\beta}\mathbf{s} \odot \mathbf{d}(\zeta) \right\| \\ &= \arg\min_{\tilde{\beta},\zeta} \left\| \mathbf{y}_1 \odot \mathbf{s}^* - \tilde{\beta}\mathbf{d}(\zeta) \right\|, \end{aligned} \tag{38}$$

where the second equality holds because $s(n)$ is constant modulus. Similar to (17), the ML estimation of ζ is

$$\begin{aligned} \hat{\zeta} &= \arg\max_{\zeta} \frac{(\mathbf{y}_1 \odot \mathbf{s}^*)^H \mathbf{d}(\zeta)\mathbf{d}^H(\zeta)(\mathbf{y}_1 \odot \mathbf{s}^*)}{\mathbf{d}^H(\zeta)\mathbf{d}(\zeta)} \\ &= \arg\max_{\zeta} \left| \mathbf{d}(\zeta)^H (\mathbf{y}_1 \odot \mathbf{s}^*) \right|^2. \end{aligned} \tag{39}$$

Noting the sinusoidal structure of $\mathbf{d}(\zeta)$ defined in (10), we see that $\mathbf{d}(\zeta)^H(\mathbf{y}_1 \odot \mathbf{s}^*)$ is the DTFT of the sequence $(\mathbf{y}_1 \odot \mathbf{s}^*)$ and thus a fast Fourier transform (FFT) can be applied to $(\mathbf{y}_1 \odot \mathbf{s}^*)$ to estimate ζ promptly.

Then take L samples corresponding to the second half of the pilot sequence

$$y_2(n) = \beta e^{-\frac{j\pi\tau^2}{\tilde{L}}} s^*(n) e^{j2\pi\left(\xi + \frac{\tau}{\tilde{L}}\right)n} + z_2(n), \tag{40}$$

and define similarly

$$\mathbf{y}_2 = [y_2(-L/2), y_2(-L/2+1), \ldots, y_2(L/2-1)]^T, \tag{41}$$

and

$$\eta \triangleq \xi + \frac{\tau}{\tilde{L}}. \tag{42}$$

Similar to (39), the ML estimation of η is

$$\hat{\eta} = \arg\max_{\eta} \left|\mathbf{d}(\eta)^H(\mathbf{y}_2 \odot \mathbf{s})\right|^2, \tag{43}$$

which can also be promptly solved by applying an FFT to $(\mathbf{y}_2 \odot \mathbf{s})$.

Combining (36) and (42) leads to the time delay and frequency offset estimates as

$$\hat{\tau} = \frac{(\hat{\eta} - \hat{\zeta})\tilde{L}}{2}, \quad \hat{\xi} = \frac{\hat{\eta} + \hat{\zeta}}{2}. \tag{44}$$

Now we see the great benefit of adopting the conjugate ZC sequences: the two-dimensional problem of jointly estimating the time delay and the frequency offset can be efficiently solved by using one-dimensional FFT twice, followed by the simple formula (44).

IV. The JEVAR in Single-Path Case

This section studies the JEVAR problem in the single-path case; the multi-path problem will be addressed in Section V.

Compared with (8), the received samples in the single-path case are

$$\mathbf{Y} = \beta\mathbf{a}(\boldsymbol{\theta})\mathbf{x}(\tau, \xi)^T + \mathbf{Z} \in \mathbb{C}^{M\times 2L}. \tag{45}$$

Since the pilot consists of two halves, we split $\mathbf{Y}$ accordingly into $\mathbf{Y} = [\mathbf{Y}_1 \vdots \mathbf{Y}_2]$, split $\mathbf{x}(\tau, \xi)^T$ into $\mathbf{x}(\tau, \xi)^T = [\mathbf{x}_1(\tau, \xi)^T \vdots \mathbf{x}_2(\tau, \xi)^T]$, and vectorize (45) into

$$\begin{bmatrix} \tilde{\mathbf{y}}_1 \\ \cdots \\ \tilde{\mathbf{y}}_2 \end{bmatrix} = \beta \begin{bmatrix} \mathbf{x}_1(\tau, \xi) \\ \cdots \\ \mathbf{x}_2(\tau, \xi) \end{bmatrix} \otimes \mathbf{a}(\theta) + \mathrm{vec}(\mathbf{Z}), \tag{46}$$

where $\tilde{\mathbf{y}}_i \triangleq \mathrm{vec}(\mathbf{Y}_i), i = 1, 2$.

In the single-path case, the JEVAR problem (17) reduces to a three-dimensional problem

$$\{\hat{\tau}, \hat{\xi}, \hat{\theta}\} = \arg\max_{\tau,\xi,\theta} \frac{\left|\begin{bmatrix} \tilde{\mathbf{y}}_1 \\ \tilde{\mathbf{y}}_2 \end{bmatrix}^H \left\{\begin{bmatrix} \mathbf{x}_1(\tau, \xi) \\ \mathbf{x}_2(\tau, \xi) \end{bmatrix} \otimes \mathbf{a}(\theta)\right\}\right|^2}{\left\|\begin{bmatrix} \mathbf{x}_1(\tau, \xi) \\ \mathbf{x}_2(\tau, \xi) \end{bmatrix} \otimes \mathbf{a}(\theta)\right\|^2}. \tag{47}$$

Since $\mathbf{x}_1(\tau, \xi)$, $\mathbf{x}_2(\tau, \xi)$, and $\mathbf{a}(\theta)$ all have unit-modulus elements, the denominator in (47) is a constant; thus, (47) can be simplified as

$$\begin{aligned} \{\hat{\tau}, \hat{\xi}, \hat{\theta}\} &= \arg\max_{\tau,\xi,\theta} \left|\begin{bmatrix} \tilde{\mathbf{y}}_1 \\ \tilde{\mathbf{y}}_2 \end{bmatrix}^H \left\{\begin{bmatrix} \mathbf{x}_1(\tau, \xi) \\ \mathbf{x}_2(\tau, \xi) \end{bmatrix} \otimes \mathbf{a}(\theta)\right\}\right|^2 \\ &= \arg\max_{\tau,\xi,\theta} \left|\tilde{\mathbf{y}}_1^H \{\mathbf{x}_1(\tau, \xi) \otimes \mathbf{a}(\theta)\} + \tilde{\mathbf{y}}_2^H \{\mathbf{x}_2(\tau, \xi) \otimes \mathbf{a}(\theta)\}\right|^2. \end{aligned} \tag{48}$$

Using the formula $[\mathrm{vec}(\mathbf{A}^H\mathbf{B}\mathbf{C}^*)]^H = [\mathrm{vec}(\mathbf{B})]^H(\mathbf{C} \otimes \mathbf{A})$, we see that

$$\tilde{\mathbf{y}}_1^H \{\mathbf{x}_1(\tau, \xi) \otimes \mathbf{a}(\theta)\} = [\mathrm{vec}(\mathbf{a}(\theta)^H\mathbf{Y}_1\mathbf{x}_1(\tau, \xi)^*)]^H. \tag{49}$$

Applying the relationship (49) to (48) leads to

$$\begin{aligned} \{\hat{\tau}, \hat{\xi}, \hat{\theta}\} = \arg\max_{\tau,\xi,\theta} \big|&\mathbf{a}(\theta)^H\mathbf{Y}_1\mathbf{x}_1(\tau, \xi)^* \\ &+ \mathbf{a}(\theta)^H\mathbf{Y}_2\mathbf{x}_2(\tau, \xi)^*\big|^2. \end{aligned} \tag{50}$$

Note that

$$\mathbf{x}_1(\tau, \xi) = \mathbf{x}(\tau) \odot \mathbf{d}(\xi) \tag{51}$$

$$= e^{j\frac{\pi\tau^2}{\tilde{L}}}\mathbf{s} \odot \mathbf{d}\left(-\frac{\tau}{\tilde{L}}\right) \odot \mathbf{d}(\xi) \tag{52}$$

$$= e^{j\frac{\pi\tau^2}{\tilde{L}}}\mathbf{s} \odot \mathbf{d}\left(\xi - \frac{\tau}{\tilde{L}}\right), \tag{53}$$

where to obtain (52) from (51) we have used (25).

Similarly,

$$\mathbf{x}_2(\tau, \xi) = \mathbf{x}^*(\tau) \odot \mathbf{d}(\xi)e^{j2\pi\xi(Q+L)} \tag{54}$$

$$= e^{-j\frac{\pi\tau^2}{\tilde{L}}}e^{j2\pi\xi(Q+L)}\mathbf{s}^* \odot \mathbf{d}\left(\frac{\tau}{\tilde{L}}\right) \odot \mathbf{d}(\xi) \tag{55}$$

$$= e^{-j\frac{\pi\tau^2}{\tilde{L}}}e^{j2\pi\xi(Q+L)}\mathbf{s}^* \odot \mathbf{d}\left(\xi + \frac{\tau}{\tilde{L}}\right), \tag{56}$$

where the term $e^{j2\pi\xi(Q+L)}$ is the phase change over the duration of the first ZC sequence plus the suffix, and the prefix of the second ZC sequence due to the frequency offset.

Inserting (51) and (54) into (50) yields

$$\begin{aligned} \{\hat{\tau}, \hat{\xi}, \hat{\theta}\} = \arg\max_{\tau,\xi,\theta} \Big|&e^{-j\frac{\pi\tau^2}{\tilde{L}}}\mathbf{a}(\theta)^H\mathbf{Y}_1\,\mathrm{diag}(\mathbf{s}^*)\mathbf{d}\left(-\xi + \frac{\tau}{\tilde{L}}\right) \\ &+ e^{j\frac{\pi\tau^2}{\tilde{L}}}e^{-j2\pi\xi(Q+L)}\mathbf{a}(\theta)^H\mathbf{Y}_2\,\mathrm{diag}(\mathbf{s})\mathbf{d}\left(-\xi - \frac{\tau}{\tilde{L}}\right)\Big|^2. \end{aligned} \tag{57}$$

Denoting

$$\tilde{\mathbf{Y}}_1 \triangleq \mathbf{Y}_1\,\mathrm{diag}(\mathbf{s}^*), \quad \tilde{\mathbf{Y}}_2 \triangleq \mathbf{Y}_2\,\mathrm{diag}(\mathbf{s}), \tag{58}$$

we simplify (57) as

$$\begin{aligned} \{\hat{\tau}, \hat{\xi}, \hat{\theta}\} = \arg\max_{\tau,\xi,\theta} \Big|&e^{-j\frac{2\pi\tau^2}{\tilde{L}}}\mathbf{a}(\theta)^H\tilde{\mathbf{Y}}_1\mathbf{d}\left(-\xi + \frac{\tau}{\tilde{L}}\right) \\ &+ e^{-j2\pi\xi(Q+L)}\,\mathbf{a}(\theta)^H\tilde{\mathbf{Y}}_2\mathbf{d}\left(-\xi - \frac{\tau}{\tilde{L}}\right)\Big|^2. \end{aligned} \tag{59}$$

The 3-dimension optimization problem (59) can be solved using a standard Newton's iterative method, given a good initialization. In the next, we present an efficient initial estimation.

A. Initial JEVAR Estimation

Using the notations ζ and η as defined in (36) and (42), we transform (59) into

$$\begin{aligned} \{\hat{\zeta}, \hat{\eta}, \hat{\theta}\} = \arg\max_{\zeta,\eta,\theta} \Big|&e^{-j\frac{\pi}{2}(\eta-\zeta)^2\tilde{L}}\mathbf{a}(\theta)^H\tilde{\mathbf{Y}}_1\mathbf{d}(-\zeta) \\ &+ e^{-j\pi(\eta+\zeta)(L+Q)}\mathbf{a}(\theta)^H\tilde{\mathbf{Y}}_2\mathbf{d}(-\eta)\Big|^2, \end{aligned} \tag{60}$$

where the two terms correspond to the two halves of the pilot.

If use only the first half pilot, then we obtain a suboptimal estimation of ζ and θ:

$$\{\hat{\zeta},\hat{\theta}\} = \arg\max_{\zeta,\theta} \left| e^{-j\frac{\pi}{2}(\eta-\zeta)^2\tilde{L}} \mathbf{a}(\theta)^H \tilde{\mathbf{Y}}_1 \mathbf{d}\left(-\zeta\right) \right|^2$$
$$= \arg\max_{\zeta,\eta,\theta} \left| \mathbf{a}(\theta)^H \tilde{\mathbf{Y}}_1 \mathbf{d}\left(-\zeta\right) \right|^2; \tag{61}$$

similarly, if use only the second half pilot, then we obtain a suboptimal estimation of η and θ:

$$\{\hat{\eta},\hat{\theta}\} = \arg\max_{\eta,\theta} \left| e^{-j\pi(\eta+\zeta)(L+Q)} \mathbf{a}(\theta)^H \tilde{\mathbf{Y}}_2 \mathbf{d}\left(-\eta\right) \right|^2$$
$$= \arg\max_{\eta,\theta} \left| \mathbf{a}(\theta)^H \tilde{\mathbf{Y}}_2 \mathbf{d}\left(-\eta\right) \right|^2. \tag{62}$$

We can estimate ζ and θ, denoted as $\hat{\theta}_1$, by applying a two-dimensional FFT (2D-FFT) to $\tilde{\mathbf{Y}}_1$ and localizing the largest entry; similarly, we can estimate η and θ, denoted as $\hat{\theta}_2$, by applying a 2D-FFT to $\tilde{\mathbf{Y}}_2$. Thus, the initial estimates are [cf. (44)]

$$\hat{\tau} = \frac{(\hat{\eta}-\hat{\zeta})\tilde{L}}{2}, \quad \hat{\xi} = \frac{\hat{\eta}+\hat{\zeta}}{2}, \quad \hat{\theta} = \frac{\hat{\theta}_1+\hat{\theta}_2}{2}. \tag{63}$$

B. Refined JEVAR Estimation

Given the initial estimation (63), we use Newton's iterative method for refined estimation of τ, ξ and θ. Let Λ denote the objective function of (59), i.e.,

$$\Lambda(\boldsymbol{\psi}) \triangleq \left| e^{-j\frac{2\pi\tau^2}{\tilde{L}}} \mathbf{a}(\theta)^H \tilde{\mathbf{Y}}_1 \mathbf{d}\left(-\xi + \frac{\tau}{\tilde{L}}\right) \right.$$
$$\left. + e^{-j2\pi\xi(Q+L)}\, \mathbf{a}(\theta)^H \tilde{\mathbf{Y}}_2 \mathbf{d}\left(-\xi - \frac{\tau}{\tilde{L}}\right) \right|^2, \tag{64}$$

where $\boldsymbol{\psi} \triangleq [\tau,\xi,\theta]^T$. After calculating the Hessian matrix $\mathbf{H} \in \mathbb{R}^{3\times 3}$ and the Jacobian vector $\mathbf{g} \in \mathbb{R}^{3\times 1}$ of $\Lambda(\boldsymbol{\psi})$ as derived in Appendix A, we can update the estimation as

$$\boldsymbol{\psi}^{(i+1)} = \boldsymbol{\psi}^{(i)} - s\mathbf{H}^{-1}\mathbf{g}, \tag{65}$$

where s is the step size determined by the backtracking line search method [34] as follows:

Set parameters $\mu = 0.3, \iota = 0.5$. Given the current value $\boldsymbol{\psi}^{(i)}$ and the searching direction $-\mathbf{H}^{-1}\mathbf{g}$, initialize the step size $s = 1$; if $\Lambda(\boldsymbol{\psi}^{(i)} - s\mathbf{H}^{-1}\mathbf{g}) < \Lambda(\boldsymbol{\psi}^{(i)}) - \mu s \mathbf{g}^T\mathbf{H}^{-1}\mathbf{g}$, then let $s = \iota s$; repeat the iteration until $\Lambda(\boldsymbol{\psi}^{(i)} - s\mathbf{H}^{-1}\mathbf{g}) \geq \Lambda(\boldsymbol{\psi}) - \mu s \mathbf{g}^T\mathbf{H}^{-1}\mathbf{g}$, then the proper step size s for (65) is obtained.

In summary, the proposed scheme for the JEVAR in the single-path scenario consists of two steps: i) to obtain the initial estimates according to (61), (62) and (63); ii) to use Newton's method (65) to search for the optimal estimation of (59). Fast convergence is guaranteed owing to the good, albeit simple, initialization of the Newton's method. We summarize the JEVAR scheme for the single-path scenario in Algorithm 1.

C. Computational Complexity

By using the conjugate ZC pair, the solution to the original three-dimensional problem (59) can be initialized via $N_\theta \times N_f$ 2D-FFTs applied to solved (61) and (62) followed by the simple algebra in (63), where N_θ is the number of grids in the angle domain and N_f is that in the frequency domain. Such FFTs incurs $O(MN_f\log_2(N_f) + N_f N_\theta \log_2(N_\theta))$ flops.

Algorithm 1: The JEVAR scheme in single-path.

Input: the received signal $\mathbf{Y}$;
Use 2D-FFTs according to (61) and (62) to estimate $\{\hat{\zeta},\hat{\theta}_1\}$ and $\{\hat{\eta},\hat{\theta}_2\}$;
Initialize the estimate $\boldsymbol{\psi}^{(0)} = \{\hat{\tau},\hat{\xi},\hat{\theta}\}$ using (63);
while not converged **do**
  Calculate $\Lambda(\boldsymbol{\psi}^{(i)})$, $\mathbf{g}$ and $\mathbf{H}$ according to (64), (89) and (101), respectively;
  Calculate s by using the backtracking line search;
  Update $\boldsymbol{\psi}^{(i+1)} = \boldsymbol{\psi}^{(i)} - s\mathbf{H}^{-1}\mathbf{g}$;
  $i = i+1$;
end while
Output: $\{\hat{\tau},\hat{\xi},\hat{\theta}\}$.

After the initialization, the refined estimation uses Newton's method (65), which is based on calculating the derivatives of the cost function $\Lambda(\boldsymbol{\psi})$ as given in Appendix A. Evaluating (64) and its derivatives takes $O(LM)$ flops, while the additional flops needed in solving $\mathbf{H}^{-1}\mathbf{g}$ is relatively minor. Since Newton's iterative method typically converges fast, the total number of flops is dominated by those of the 2D-FFTs, that is, $O(MN_f\log_2(N_f) + N_f N_\theta \log_2(N_\theta))$.

In contrast, a state-of-the-art approach, e.g., the one in [25] uses an initialization of the JEVAR estimate requiring $O(N_\tau M N_f \log_2 N_f)$ flops, where N_τ is the number of search grid points in time domain, which can be large when the time delay range is large (e.g., $N_\tau = 200$ for a delay range of $100T_s$ with time grid interval $0.5T_s$. Compared $O(MN_f\log_2(N_f) + N_f N_\theta \log_2(N_\theta))$ with $O(N_\tau M N_f \log_2 N_f)$, the proposed method can be at least one order of magnitude faster thanks to adopting the conjugate pair of ZCs as the pilot.

D. The Closed-Form CRB

We have derived the CRB of the JEVAR estimation in the closed-form as

$$CRB(\tau) = \frac{4\pi^2}{3}\cdot\gamma^{-1}\cdot\frac{\tilde{L}^2}{L^2-1}, \tag{66}$$

$$CRB(\xi) = \frac{4\pi^2}{3}\cdot\gamma^{-1}\cdot\frac{1}{4\,L^2+6LQ+3Q^2}, \tag{67}$$

$$CRB(\theta) = \frac{4\pi^2}{3}\cdot\gamma^{-1}\cdot\frac{(\lambda/d)^2}{(M^2-1)\cos^2\theta}, \tag{68}$$

for $\tau \approx 0$, where $\gamma = \frac{|\beta|^2 ML}{\sigma^2}$. The derivations are straightforward and are omitted due to page limitation.

As γ is the input signal-to-noise ratio (SNR) times the processing gain ML, it is intuitively pleasing to see that all the CRBs are inversely proportional to γ. It is also interesting to note that the precision of AOA estimation is (roughly) proportional to $M^3\,L$, and the precision of frequency offset estimation is (roughly) proportional to ML^3, while the delay estimation accuracy is only proportional to ML since $\frac{\tilde{L}^2}{L^2-1}$ is a constant.

V. The JEVAR in Multipath Case

This section proceeds to study the multipath case. The key idea is to use the AP method [29], [35] to decompose the multipaths into multiple single paths, to which the method in the previous section can be applied multiple times.

Compared with (45), the received samples in the multipath case are

$$\mathbf{Y} = \mathbf{A}(\boldsymbol{\theta})\,\mathrm{diag}(\boldsymbol{\beta})\mathbf{X}(\boldsymbol{\tau},\boldsymbol{\xi})^T + \mathbf{Z}. \tag{69}$$

Applying the same algebraic manipulation that leads from (45) to (46), we can obtain from (69) that

$$\begin{bmatrix} \tilde{\mathbf{y}}_1 \\ \cdots \\ \tilde{\mathbf{y}}_2 \end{bmatrix} = \sum_{u=1}^{U} \beta_u \begin{bmatrix} \mathbf{x}_1(\tau_u,\xi_u) \\ \cdots \\ \mathbf{x}_2(\tau_u,\xi_u) \end{bmatrix} \otimes \mathbf{a}(\theta_u) + \mathrm{vec}(\mathbf{Z}). \tag{70}$$

where $\mathbf{x}_1$ and $\mathbf{x}_2$ are as defined in (51) and (54).

Denote

$$\tilde{\mathbf{y}} = \begin{bmatrix} \tilde{\mathbf{y}}_1 \\ \cdots \\ \tilde{\mathbf{y}}_2 \end{bmatrix} \in \mathbb{C}^{2LM\times 1}, \tag{71}$$

$$\tilde{\mathbf{x}}_u \triangleq \begin{bmatrix} \mathbf{x}_1(\tau_u,\xi_u) \\ \cdots \\ \mathbf{x}_2(\tau_u,\xi_u) \end{bmatrix} \otimes \mathbf{a}(\theta_u) \in \mathbb{C}^{2LM\times 1}, \tag{72}$$

$$\tilde{\mathbf{X}} = [\tilde{\mathbf{x}}_1,\ldots,\tilde{\mathbf{x}}_u,\ldots,\tilde{\mathbf{x}}_U] \in \mathbb{C}^{2LM\times U}, \tag{73}$$

and $\tilde{\mathbf{X}}_u \in \mathbb{C}^{2LM\times(U-1)}$ as obtained by striking $\tilde{\mathbf{x}}_u$ from $\tilde{\mathbf{X}}$. By utilizing the properties of projection matrix [36], we have the orthogonal projection matrix of $\tilde{\mathbf{X}}$:

$$\mathcal{P}(\tilde{\mathbf{X}}) = \mathcal{P}(\tilde{\mathbf{X}}_u) + \mathcal{P}\left\{\mathcal{P}^{\perp}(\tilde{\mathbf{X}}_u)\tilde{\mathbf{x}}_u\right\}, \tag{74}$$

where $\mathcal{P}^{\perp}(\tilde{\mathbf{X}}_u) = \mathbf{I} - \mathcal{P}(\tilde{\mathbf{X}}_u)$. Inserting (74) into the objective function of (17), we obtain

$$\{\hat{\boldsymbol{\tau}},\hat{\boldsymbol{\xi}},\hat{\boldsymbol{\theta}}\} = \arg\max_{\boldsymbol{\tau},\boldsymbol{\xi},\boldsymbol{\theta}} \tilde{\mathbf{y}}^H \left[\mathcal{P}(\tilde{\mathbf{X}}_u) + \mathcal{P}\{\mathcal{P}^{\perp}(\tilde{\mathbf{X}}_u)\tilde{\mathbf{x}}_u\}\right]\tilde{\mathbf{y}}. \tag{75}$$

Given that $\tilde{\mathbf{X}}_u$ is known and fixed (i.e., $\{\tau_k,\xi_k,\theta_k\}_{k=1,k\neq u}^{U}$ are known), (75) can be simplified as

$$\begin{aligned}\{\hat{\tau}_u,\hat{\xi}_u,\hat{\theta}_u\} &= \arg\max_{\tau_u,\xi_u,\theta_u} \tilde{\mathbf{y}}^H \mathcal{P}\left\{\mathcal{P}^{\perp}(\tilde{\mathbf{X}}_u)\tilde{\mathbf{x}}_u\right\}\tilde{\mathbf{y}} \\ &= \arg\max_{\tau_u,\xi_u,\theta_u} \frac{\left|\tilde{\mathbf{y}}^H\mathcal{P}^{\perp}(\tilde{\mathbf{X}}_u)\tilde{\mathbf{x}}_u\right|^2}{\tilde{\mathbf{x}}_u^H\mathcal{P}^{\perp}(\tilde{\mathbf{X}}_u)\tilde{\mathbf{x}}_u};\end{aligned} \tag{76}$$

thus, the AP decomposes the multipath problem into multiple single paths.

We approximate the initial estimate of the u^{th} path as

$$\begin{aligned}\{\hat{\tau}_u,\hat{\xi}_u,\hat{\theta}_u\} &\approx \arg\max_{\tau_u,\xi_u,\theta_u} \frac{\left|\tilde{\mathbf{y}}^H\mathcal{P}^{\perp}(\tilde{\mathbf{X}}_u)\tilde{\mathbf{x}}_u\right|^2}{\tilde{\mathbf{x}}_u^H\tilde{\mathbf{x}}_u} \\ &= \arg\max_{\tau_u,\xi_u,\theta_u} \left|\tilde{\mathbf{y}}^H\mathcal{P}^{\perp}(\tilde{\mathbf{X}}_u)\tilde{\mathbf{x}}_u\right|^2,\end{aligned} \tag{77}$$

Algorithm 2: The JEVAR scheme in multipath.

Input: the number of multipath U and the received signal $\tilde{\mathbf{y}}$;
Estimate $\{\hat{\tau}_1,\hat{\xi}_1,\hat{\theta}_1\}$ via (79) using Algorithm 1;
for $u = 2:U$ **do**
  Update $\tilde{\mathbf{X}}_u = [\tilde{\mathbf{x}}_1,\ldots,\tilde{\mathbf{x}}_{u-1}]$;
  Solve (77) using 2D-FFTs and apply (63) to obtain the initial estimate of $\{\hat{\tau}_u,\hat{\xi}_u,\hat{\theta}_u\}$;
  Solve (76) using the Newton's method (65) to obtain the refined estimate of $\{\hat{\tau}_u,\hat{\xi}_u,\hat{\theta}_u\}$;
end for
while not converged **do**
  for $u = 1:U$ **do**
    Update $\tilde{\mathbf{X}}_u = [\tilde{\mathbf{x}}_1,\ldots,\tilde{\mathbf{x}}_{u-1},\tilde{\mathbf{x}}_{u+1},\ldots,\tilde{\mathbf{x}}_U]$;
    Solve (77) using 2D-FFTs and apply (63) to obtain the initial estimate of $\{\hat{\tau}_u,\hat{\xi}_u,\hat{\theta}_u\}$;
    Solve (76) using the Newton's method (65) to obtain the refined estimate of $\{\hat{\tau}_u,\hat{\xi}_u,\hat{\theta}_u\}$;
  end for
end while
Output: $\{\hat{\boldsymbol{\tau}},\hat{\boldsymbol{\xi}},\hat{\boldsymbol{\theta}}\}$.

which can be solved the same way as presented in Section IV, before applying Newton's method to (76) for the refined estimation.

In the scenario where two paths have similar gains, it is likely that the parameters obtained from the two half pilots [cf. (61) and (62)] correspond to different reflections. To make sure the estimates from the two half ZCs are associated with the same path, after solving (61) and obtaining $\hat{\theta}_u$, we estimate η as

$$\hat{\eta}_u = \arg\max_{\eta_u} \left|\mathbf{a}(\hat{\theta}_u)^H\tilde{\mathbf{Y}}_2\mathbf{d}\left(-\eta_u\right)\right|^2, \tag{78}$$

which is the same as (62) except for setting θ to be $\hat{\theta}_u$.

To initialize the AP procedure, we assume the received signal contains only one path and estimate $\{\hat{\tau}_1,\hat{\xi}_1,\hat{\theta}_1\}^{(1)}$ via

$$\{\hat{\tau}_1,\hat{\xi}_1,\hat{\theta}_1\}^{(1)} = \arg\max_{\tau_1,\xi_1,\theta_1} \left|\tilde{\mathbf{y}}^H\tilde{\mathbf{x}}_1\right|^2, \tag{79}$$

where the superscript denotes the iteration index;

thus $\tilde{\mathbf{x}}_1^{(1)} = \mathbf{x}(\tau_1,\xi_1)\otimes\mathbf{a}(\theta_1)$ is obtained. Then we set $\tilde{\mathbf{X}}_2 = \tilde{\mathbf{x}}_1^{(1)}$ and estimate $\{\hat{\tau}_2,\hat{\xi}_2,\hat{\theta}_2\}^{(1)}$ from (77). Next we set $\tilde{\mathbf{X}}_3 = [\tilde{\mathbf{x}}_1^{(1)},\tilde{\mathbf{x}}_2^{(1)}]$ and estimate $\{\hat{\tau}_3,\hat{\xi}_3,\hat{\theta}_3\}^{(1)}$. This procedure continues until $\{\hat{\tau}_U,\hat{\xi}_U,\hat{\theta}_U\}^{(1)}$ with $\tilde{\mathbf{X}}_U = [\tilde{\mathbf{x}}_1^{(1)},\tilde{\mathbf{x}}_2^{(1)},\ldots,\tilde{\mathbf{x}}_{U-1}^{(1)}]$.

In the second round of iteration, first estimate $\{\hat{\tau}_1,\hat{\xi}_1,\hat{\theta}_1\}^{(2)}$ according to (76) with $\tilde{\mathbf{X}}_1 = [\tilde{\mathbf{x}}_2^{(1)},\tilde{\mathbf{x}}_3^{(1)},\ldots,\tilde{\mathbf{x}}_U^{(1)}]$. Then estimate $\{\hat{\tau}_2,\hat{\xi}_2,\hat{\theta}_2\}^{(2)}$ according to (76) with $\tilde{\mathbf{X}}_2 = [\tilde{\mathbf{x}}_1^{(2)},\tilde{\mathbf{x}}_3^{(1)},\ldots,\tilde{\mathbf{x}}_U^{(1)}]$, and so on. Proceed the iterations to update the parameters of each path until convergence. We summarize the JEVAR scheme for the multipath scenario in Algorithm 2.

Remark 1: Besides the aforementioned AP method, the classic SAGE method [24] can also be applied to decompose the multipath problem to multiple single-path subproblems. The

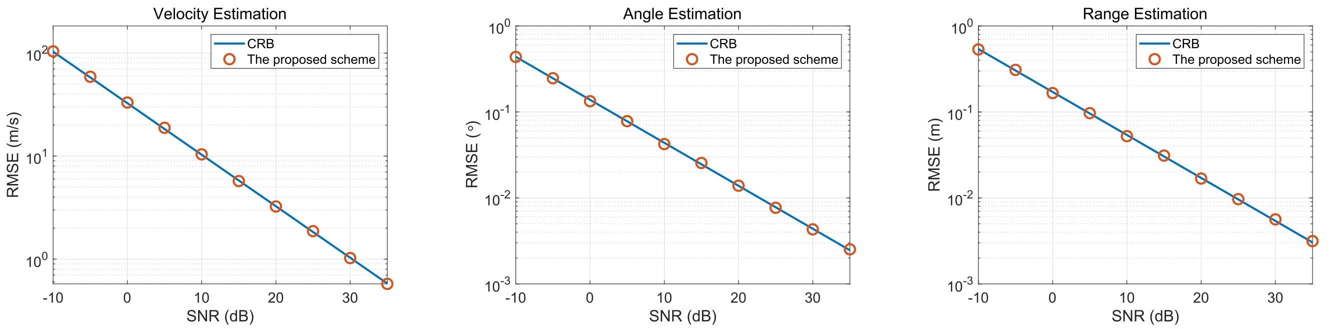

Fig. 7. The RMSEs of the velocity, angle and range estimation in the single-path case compared with the CRBs.

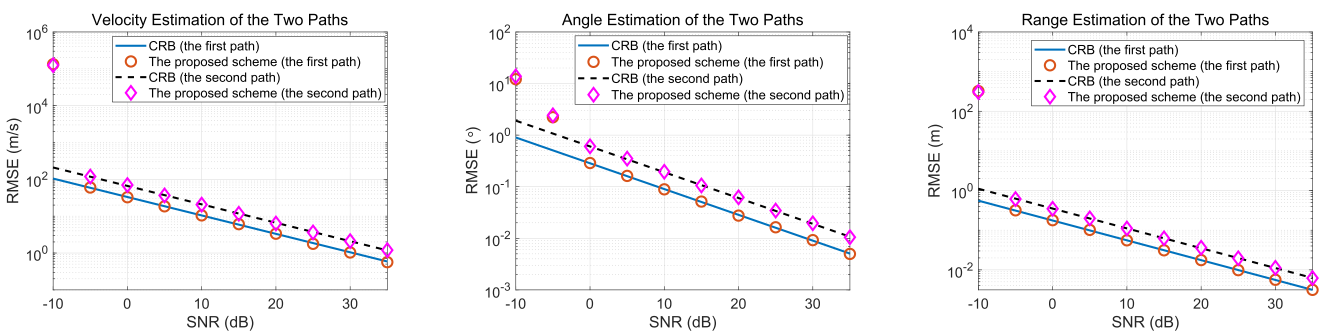

Fig. 8. The RMSEs of the velocity, angle and range estimation in the two-path case compared with the CRBs.

SAGE consists of two steps : the expectation step (E-step), which calculates

$$\hat{\tilde{\mathbf{y}}}_u = \tilde{\mathbf{y}} - \sum_{\substack{i=1 \\ i \neq u}}^{U} \beta_i \tilde{\mathbf{x}}_i, \tag{80}$$

where $\tilde{\mathbf{x}}_i$ is as defined in (72), and the M-step, which calculates

$$\{\hat{\tau}_u, \hat{\xi}_u, \hat{\theta}_u\} = \arg \max_{\tau_u, \xi_u, \theta_u} |\hat{\tilde{\mathbf{y}}}_u^H \tilde{\mathbf{x}}_u|^2, \tag{81}$$

and

$$\hat{\beta}_u = (\hat{\tilde{\mathbf{x}}}_u^H \hat{\tilde{\mathbf{x}}}_u)^{-1} \hat{\tilde{\mathbf{x}}}_u^H \hat{\tilde{\mathbf{y}}}_u. \tag{82}$$

Similar to the AP method, the SAGE method estimates parameters of each path iteratively until convergence. Although the AP method in one iteration is more computationally complicated than the SAGE method, as it needs the calculation of the projection matrix calculation, it can significantly outperform the SAGE method in resolving closely-spaced multipaths, as we will show in the next section.

VI. Simulation Results

This section evaluates the performance of the proposed scheme through numerical simulations. Consider a 6-antenna ULA with half wavelength inter-element spacing. The transmitted pilot is the concatenation of a pair of conjugate ZC sequences of length $L = 250$ and $\tilde{L} = 400$, each with a length-15 prefix and a length-15 suffix, i.e., $Q = 30$. The pulse shaper is a raised cosine filter with the roll-off factor $\alpha = 0.3$. The carrier frequency $f_c = 2.4$ GHz and the bandwidth $B = 20$ MHz, that is, the Nyquist sampling interval is $T_s = 50$ns. Each simulation result is based on 1000 Monte-Carlo trials.

We first simulate the single-path LOS scenario, where the AOA $\theta = 5^\circ$, the Doppler frequency offset $\xi = 3 \times 10^{-5}/T_s$ (or 600 Hz), the time delay $\tau = 1.2T_s$, and the channel complex gain $\beta = e^{j\phi}$ with ϕ being random. The propagation distance and radial velocity is $\rho = 18$ m and $v = 75$ m/s. Fig. 7 shows the root mean square errors (RMSEs) estimation of the velocity, angle and range versus SNR. We can see that the RMSE results of the proposed scheme almost overlap with the CRBs as derived in Appendix B. At the SNR 20 dB, the RMSE of the range estimation is about 2 cm, which is a striking result given only 20 MHz bandwidth; the velocity estimation error is about 3 m/s, and the angle estimation error is only 0.01°. Here we have used the range-delay translation $\rho = \tau \times C$, and the velocity-Doppler frequency offset translation $v = \frac{C\xi}{f_c}$.

Then we evaluate the JEVAR's super-resolution capability of differentiating two paths that are closely-spaced in the time domain. Consider a two-path case where $\boldsymbol{\xi} = [3 \times 10^{-5}, 7 \times 10^{-5}]/T_s$, $\boldsymbol{\theta} = [5^\circ, 20^\circ]$, $\boldsymbol{\tau} = [1.2, 1.3]T_s$, and $\boldsymbol{\beta} = [e^{j\phi_1}, 0.5e^{j\phi_2}]$ with ϕ_1 and ϕ_2 being random. The propagation distance and radial velocity of the two-path are $\boldsymbol{\rho} = [18, 19.5]$m and $\boldsymbol{v} = [75, 175]$m/s, respectively. The convergence for the AP is reached if $|\tau_u^{(k)} - \tau_u^{(k-1)}| < 10^{-5}T_s$, $|\xi_u^{(k)} - \xi_u^{(k-1)}| < 10^{-8}/T_s$, $|\theta_u^{(k)} - \theta_u^{(k-1)}| < 10^{-4\circ}$, or $k > 30$, where k denotes the k^{th} iteration. The convergence conditions are set to be at least two order of magnitude lower than the CRBs of the parameters.

Fig. 8 shows the RMSEs estimation of the velocities, angles and ranges of the two paths, compared with their respective CRBs. These results verify the JEVAR's super-resolution capability to separate two closely spaced multipaths.

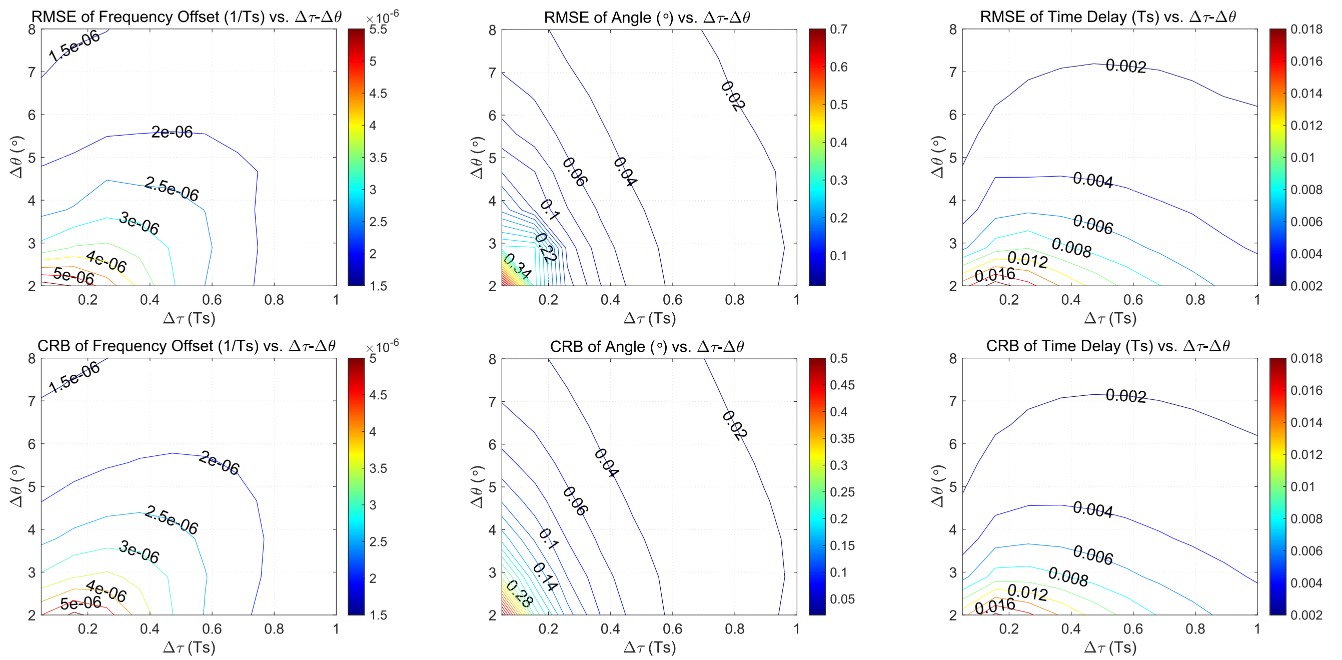

Fig. 9. The first row of the pictures shows the RMSEs of frequency offset, angle and time delay of the first path versus angle separation $\Delta\theta$ and delay separation $\Delta\tau$. The second row shows the CRBs of frequency offset, angle and time delay of the first path.

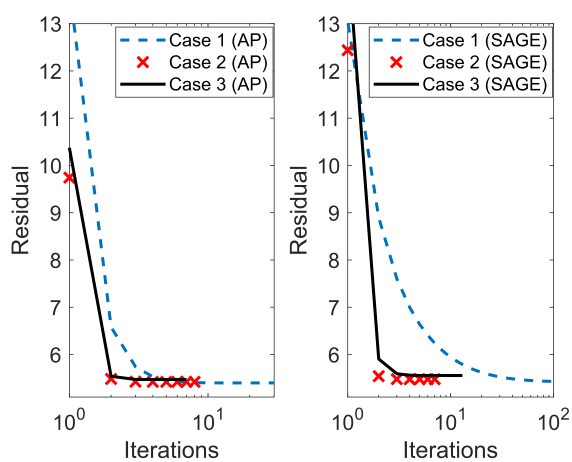

Fig. 10. Convergence behaviors of the AP and the SAGE under different multipath settings.

The third example simulates the proposed scheme in the environment with two equal-power paths whose $\boldsymbol{\xi} = [10^{-5}, 10^{-5}]/T_s$, $\boldsymbol{\theta} = [10^\circ, 10^\circ + \Delta\theta]$ and $\boldsymbol{\tau} = [1.1, 1.1 + \Delta\tau]T_s$. The SNR is 20 dB. The upper three subplots in Fig. 9 show the RMSEs of the frequency offset, angle, and time delay estimation of the first path with varying time different $\Delta\tau$ and angle difference $\Delta\theta$ between the paths, while the three lower subplots show the corresponding CRBs. Examining the contour plots we see that the proposed scheme can exploit the differentiation in both spatial and temporal domain to resolve the multipaths and can approach the CRB performance limit even in the adverse environment.

The fourth example shows the convergence performance of the AP and the SAGE. The simulated channel has two equal-power paths with $\boldsymbol{\xi} = [10^{-6}, 5 \times 10^{-5}]/T_s$. Three cases are simulated: case 1: both angles and time delays are closely spaced, where $\boldsymbol{\tau} = [0.2, 0.25]T_s$ and $\boldsymbol{\theta} = [20^\circ, 30^\circ]$; case 2: only angles are closely spaced, where $\boldsymbol{\tau} = [0.2, 2.2]T_s$ and $\boldsymbol{\theta} = [20^\circ, 30^\circ]$; case 3: only time delays are closely spaced, where $\boldsymbol{\tau} = [0.2, 0.25]T_s$ and $\boldsymbol{\theta} = [20^\circ, 45^\circ]$. Fig. 10 presents the convergence behavior at SNR $= 20$ dB according to (15), which shows that the iterative algorithms both converge faster (within several iterations) when the two paths get more separated in either spatial domain or temporal domain, or both. However, the AP method can converge significantly faster than the SAGE method in the harsh environment where the angles and time delays are both closely spaced.

The fifth example simulates a harsh environment where two equal-power paths have frequency offsets $\boldsymbol{\xi} = [10^{-5}, 10^{-4}]/T_s$, AOAs $\boldsymbol{\theta} = [10^\circ, 15^\circ]$, and time delays $\boldsymbol{\tau} = [1.1, 1.1 + \Delta\tau]T_s$. The SNR is 20 dB. Fig. 11 compares the RMSEs of the frequency offset, angle, and time delay estimates of the first path with varying time delay gap $\Delta\tau$ between the paths. Viewing that the slow convergence performance of the SAGE method in the harsh environment, we simulate the SAGE method with the maximum iterations $\kappa = 50$, 200 and 1000, while κ is 30 for the AP method. Fig. 11 indicates that the AP method can achieve the CRB and outperforms the SAGE method in this multipath environment, although the performance of the SAGE can be improved by running (many) more iterations. Take $\Delta\tau = 0.25T_s$ for example, by using the SAGE method ($\kappa = 200$), the RMSEs of the frequency offset, angle and time delay estimation are about $2 \times 10^{-5}/T_s$ (corresponding to 50 m/s velocity error), 1.1° and $0.06T_s$ (corresponding to 90 cm ranging error); in contrast, the

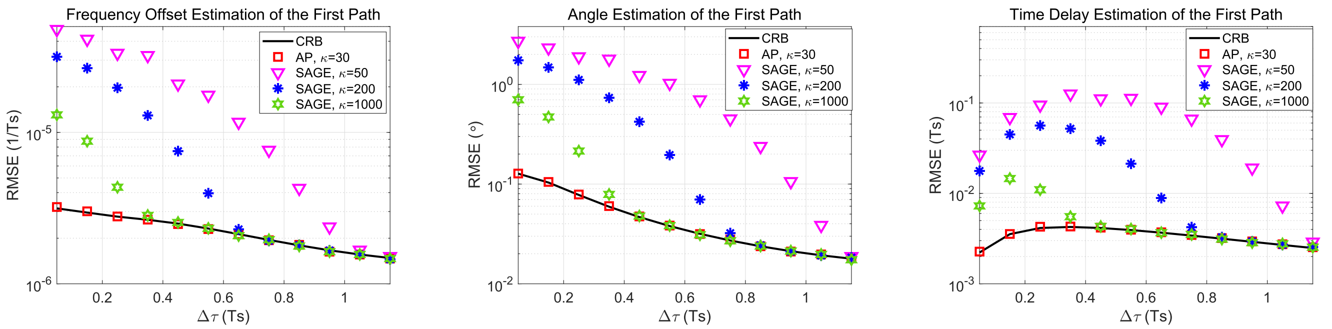

Fig. 11. Performance comparison between the AP with the SAGE in RMSEs of the LOS signal of the frequency offset, angle and time delay under different delay separation $\Delta\tau$; κ is the maximum iterations constraint for the iterative algorithms.

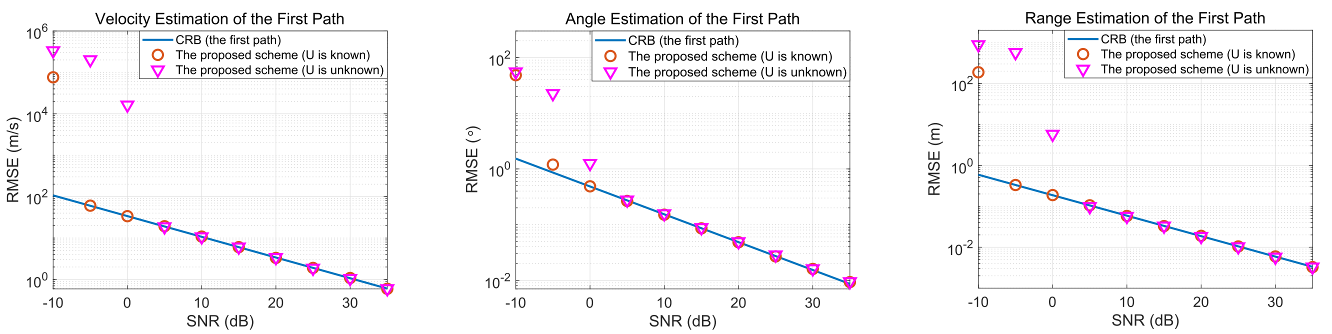

Fig. 12. RMSEs of the velocity, angle and range of the LOS signal of a four-path case.

AP method ($\kappa = 30$) yields the RMSEs of the frequency offset, angle and time delay are about $2.8 \times 10^{-6}/T_s$ (corresponding to 7 m/s velocity error), 0.08° and $4 \times 10^{-3}T_s$ (corresponding to 6 cm ranging error).

The last example simulates a four-path channel where the four equal-power paths have $\boldsymbol{\xi} = [5 \times 10^{-6}, 3 \times 10^{-5}, 1 \times 10^{-6}, 2 \times 10^{-4}]/T_s$, $\boldsymbol{\theta} = [0^\circ, 15^\circ, -25^\circ, 30^\circ]$, and $\boldsymbol{\tau} = [1.5, 1.6, 2, 3.2]T_s$. The radial velocity and propagation distance of the LOS signal is $v_1 = 12.5$ m/s and $\rho_1 = 22.5$ m. In this case, we assume that he number of multipaths U is unknown. We adopt the minimum description length criterion [31], [32] to estimate U:

$$\mathrm{MDL}(\tilde{U}) = -\log f(\mathbf{Y}|\hat{\boldsymbol{\Theta}}^{(\tilde{U})}) + \frac{5}{2}\tilde{U}\log 2L, \tag{83}$$

where $\mathbf{Y}$ is the received signal, $\tilde{U}$ is the candidate number of multipath, $\hat{\boldsymbol{\Theta}}^{(\tilde{U})} = \{\mathrm{Re}\{\hat{\boldsymbol{\beta}}\}, \mathrm{Im}\{\hat{\boldsymbol{\beta}}\}, \hat{\boldsymbol{\tau}}, \hat{\boldsymbol{\xi}}, \hat{\boldsymbol{\theta}}\} \in \mathbb{R}^{5\tilde{U}}$ is the ML estimate of the parameters, and $f(\cdot)$ is the probability density. The number of multipath is obtained by calculating the minimum of (83) with respect to $\tilde{U}$. The RMSEs of the velocity, angle, and range estimation of the LOS signal are plotted in Fig. 12, which shows that with the estimated U, the RMSEs can still approach the CRBs when SNR ≥ 0 dB.

VII. Conclusion

In this paper, we studied the joint estimation of the velocity, angle and range (JEVAR) of a target in a multipath environment, and introduced an efficient scheme – we have the target transmit a pair of conjugate ZC sequences and let the multi-antenna receiver conduct maximum likelihood (ML) estimation. Based on the alternating projection (AP) method, the multipath parameters estimation problem is transformed into multiple single-path problems. For the single-path estimation, the ambiguity property of the ZC sequences is utilized to facilitate the estimation of the time delay and frequency offset. Extensive simulations verify the superior performance of the proposed algorithm even in dense multipath case. In particular, using a waveform of 20 MHz bandwidth, the proposed scheme can achieve super resolution estimation of the range, AOA and velocity of the target, which can be very helpful for the localization and navigation related Internet of Things (IoT) applications.

Appendix A
Derivation of the Jacobian Vector and Hessian Matrix

According to (64), the objective function $\Lambda(\boldsymbol{\psi})$ of $\boldsymbol{\psi} \triangleq [\tau, \xi, \theta]^T$ can be rewritten as

$$\begin{aligned}\Lambda(\boldsymbol{\psi}) &= \left|\breve{\mathbf{y}}^H \left\{\begin{bmatrix} e^{j\frac{\pi\tau^2}{L}}\mathbf{d}(\xi - \frac{\tau}{L}) \\ e^{-j\frac{\pi\tau^2}{L}}\mathbf{d}(\xi + \frac{\tau}{L})e^{j2\pi\xi(Q+L)} \end{bmatrix} \otimes \mathbf{a}(\theta)\right\}\right|^2 \\ &= \left|\breve{\mathbf{y}}^H\breve{\mathbf{x}}\right|^2, \end{aligned} \tag{84}$$

where

$$\breve{\mathbf{y}} = \mathrm{vec}([\tilde{\mathbf{Y}}_1 \vdots \tilde{\mathbf{Y}}_2]), \tag{85}$$

$$\breve{\mathbf{x}} = \left[\breve{\mathbf{s}}(\tau) \odot \breve{\mathbf{d}}(\xi)\right] \otimes \mathbf{a}(\theta), \tag{86}$$

where

$$\breve{\mathbf{s}}(\tau) = \begin{bmatrix} e^{j\frac{\pi\tau^2}{L}}\mathbf{d}(-\frac{\tau}{L}) \\ e^{-j\frac{\pi\tau^2}{L}}\mathbf{d}(\frac{\tau}{L}) \end{bmatrix}, \tag{87}$$

$$\breve{\mathbf{d}}(\xi) = \begin{bmatrix} \mathbf{d}(\xi) \\ \mathbf{d}(\xi)e^{j2\pi\xi(Q+L)} \end{bmatrix}. \tag{88}$$

Then we will derive the Jacobian vector $\mathbf{g}$ and Hessian matrix $\mathbf{H}$ of the single path case. The Jacobian vector is expressed as

$$\mathbf{g} = \left[\frac{\partial\Lambda(\boldsymbol{\psi})}{\partial\tau}, \frac{\partial\Lambda(\boldsymbol{\psi})}{\partial\xi}, \frac{\partial\Lambda(\boldsymbol{\psi})}{\partial\theta}\right]^T, \tag{89}$$

where

$$\frac{\partial\Lambda(\boldsymbol{\psi})}{\partial\tau} = 2\,\mathrm{Re}\left\{\frac{\partial\breve{\mathbf{x}}^H}{\partial\tau}\breve{\mathbf{y}}\breve{\mathbf{y}}^H\breve{\mathbf{x}}\right\}, \tag{90}$$

$$\frac{\partial\Lambda(\boldsymbol{\psi})}{\partial\xi} = 2\,\mathrm{Re}\left\{\frac{\partial\breve{\mathbf{x}}^H}{\partial\xi}\breve{\mathbf{y}}\breve{\mathbf{y}}^H\breve{\mathbf{x}}\right\}, \tag{91}$$

$$\frac{\partial\Lambda(\boldsymbol{\psi})}{\partial\theta} = 2\,\mathrm{Re}\left\{\frac{\partial\breve{\mathbf{x}}^H}{\partial\xi}\breve{\mathbf{y}}\breve{\mathbf{y}}^H\breve{\mathbf{x}}\right\}, \tag{92}$$

where $\frac{\partial\breve{\mathbf{x}}}{\partial\tau}$, $\frac{\partial\breve{\mathbf{x}}}{\partial\xi}$ and $\frac{\partial\breve{\mathbf{x}}}{\partial\theta}$ are derived as follows.

$$\frac{\partial\breve{\mathbf{x}}}{\partial\tau} = \left[\frac{\partial\breve{\mathbf{s}}(\tau)}{\partial\tau}\odot\breve{\mathbf{d}}(\xi)\right]\otimes\mathbf{a}(\theta), \tag{93}$$

where

$$\frac{\partial\breve{\mathbf{s}}(\tau)}{\partial\tau} = \begin{bmatrix} 2j\pi\frac{\tau}{L}\cdot\mathbf{1}_L + \mathbf{d}(-\frac{1}{L}) \\ -2j\pi\frac{\tau}{L}\cdot\mathbf{1}_L + \mathbf{d}(\frac{1}{L}) \end{bmatrix}\odot\breve{\mathbf{s}}(\tau), \tag{94}$$

$$\frac{\partial\breve{\mathbf{x}}}{\partial\xi} = \left[\breve{\mathbf{s}}(\tau)\odot\frac{\partial\breve{\mathbf{d}}(\xi)}{\partial\xi}\right]\otimes\mathbf{a}(\theta), \tag{95}$$

where

$$\frac{\partial\breve{\mathbf{s}}(\tau)}{\partial\xi} = \overline{\mathbf{d}}\odot\breve{\mathbf{d}}(\xi), \tag{96}$$

and

$$\overline{\mathbf{d}} = j2\pi\,[0, 1, \ldots, L-1, L+Q, L+Q+1, \ldots, 2L+Q-1]^T, \tag{97}$$

$$\frac{\partial\tilde{\mathbf{x}}}{\partial\theta} = \left[\breve{\mathbf{s}}(\tau)\odot\breve{\mathbf{d}}(\xi)\right]\otimes\frac{\partial\mathbf{a}(\theta)}{\partial\theta}, \tag{98}$$

where

$$\frac{\partial\mathbf{a}(\theta)}{\partial\theta} = \overline{\mathbf{a}}(\theta)\odot\mathbf{a}(\theta), \tag{99}$$

and

$$\overline{\mathbf{a}}(\theta) = -\frac{2j\pi d\cos\theta}{\lambda}\,[0, 1, \ldots, M-1]^T. \tag{100}$$

The Hessian matrix can be expressed as

$$\mathbf{H} = \begin{bmatrix} \frac{\partial^2\Lambda(\boldsymbol{\psi})}{\partial\tau^2} & \frac{\partial^2\Lambda(\boldsymbol{\psi})}{\partial\tau\partial\xi} & \frac{\partial^2\Lambda(\boldsymbol{\psi})}{\partial\tau\partial\theta} \\ \frac{\partial^2\Lambda(\boldsymbol{\psi})}{\partial\xi\partial\tau} & \frac{\partial^2\Lambda(\boldsymbol{\psi})}{\partial\xi^2} & \frac{\partial^2\Lambda(\boldsymbol{\psi})}{\partial\xi\partial\theta} \\ \frac{\partial^2\Lambda(\boldsymbol{\psi})}{\partial\theta\partial\tau} & \frac{\partial^2\Lambda(\boldsymbol{\psi})}{\partial\theta\partial\xi} & \frac{\partial^2\Lambda(\boldsymbol{\psi})}{\partial\theta^2} \end{bmatrix}, \tag{101}$$

where

$$\frac{\partial^2\Lambda(\boldsymbol{\psi})}{\partial\tau^2} = 2\left|\breve{\mathbf{y}}^H\frac{\partial\breve{\mathbf{x}}}{\partial\tau}\right|^2 + 2\,\mathrm{Re}\left\{\frac{\partial^2\breve{\mathbf{x}}^H}{\partial\tau^2}\breve{\mathbf{y}}\breve{\mathbf{y}}^H\breve{\mathbf{x}}\right\}, \tag{102}$$

$$\frac{\partial^2\Lambda(\boldsymbol{\psi})}{\partial\xi^2} = 2\left|\breve{\mathbf{y}}^H\frac{\partial\breve{\mathbf{x}}}{\partial\xi}\right|^2 + 2\,\mathrm{Re}\left\{\frac{\partial^2\breve{\mathbf{x}}^H}{\partial\xi^2}\breve{\mathbf{y}}\breve{\mathbf{y}}^H\breve{\mathbf{x}}\right\}, \tag{103}$$

$$\frac{\partial^2\Lambda(\boldsymbol{\psi})}{\partial\theta^2} = 2\left|\breve{\mathbf{y}}^H\frac{\partial\breve{\mathbf{x}}}{\partial\theta}\right|^2 + 2\,\mathrm{Re}\left\{\frac{\partial^2\breve{\mathbf{x}}^H}{\partial\theta^2}\breve{\mathbf{y}}\breve{\mathbf{y}}^H\breve{\mathbf{x}}\right\}. \tag{104}$$

Besides, $\frac{\partial^2\breve{\mathbf{x}}}{\partial\tau^2}$, $\frac{\partial^2\breve{\mathbf{x}}}{\partial\xi^2}$ and $\frac{\partial^2\breve{\mathbf{x}}}{\partial\theta^2}$ are derived as follows:

$$\frac{\partial^2\breve{\mathbf{x}}}{\partial\tau^2} = \left[\frac{\partial^2\breve{\mathbf{s}}(\tau)}{\partial\tau^2}\odot\breve{\mathbf{d}}(\xi)\right]\otimes\mathbf{a}(\theta), \tag{105}$$

where

$$\frac{\partial^2\breve{\mathbf{s}}(\tau)}{\partial\tau^2} = \begin{bmatrix} 2j\pi\frac{1}{L}\cdot\mathbf{1}_L \\ -2j\pi\frac{1}{L}\cdot\mathbf{1}_L \end{bmatrix}\odot\breve{\mathbf{s}}(\tau) + \begin{bmatrix} 2j\pi\frac{\tau}{L}\cdot\mathbf{1}_L + \mathbf{d}(-\frac{1}{L}) \\ -2j\pi\frac{\tau}{L}\cdot\mathbf{1}_L + \mathbf{d}(\frac{1}{L}) \end{bmatrix}\odot\frac{\partial\breve{\mathbf{s}}}{\partial\tau}, \tag{106}$$

$$\frac{\partial^2\breve{\mathbf{x}}}{\partial\xi^2} = \left[\breve{\mathbf{s}}(\tau)\odot\frac{\partial^2\breve{\mathbf{d}}(\xi)}{\partial\xi^2}\right]\otimes\mathbf{a}(\theta), \tag{107}$$

where

$$\frac{\partial^2\breve{\mathbf{d}}(\xi)}{\partial\xi^2} = \overline{\mathbf{d}}\odot\frac{\partial\breve{\mathbf{d}}(\xi)}{\partial\xi}, \tag{108}$$

$$\frac{\partial^2\tilde{\mathbf{x}}}{\partial\theta^2} = \left[\breve{\mathbf{s}}(\tau)\odot\breve{\mathbf{d}}(\xi)\right]\otimes\frac{\partial^2\mathbf{a}(\theta)}{\partial\theta^2}, \tag{109}$$

where

$$\frac{\partial^2\mathbf{a}(\theta)}{\partial\theta^2} = (\tilde{\mathbf{a}}(\theta) + \overline{\mathbf{a}}(\theta)\odot\overline{\mathbf{a}}(\theta))\odot\mathbf{a}(\theta), \tag{110}$$

$$\tilde{\mathbf{a}}(\theta) = j\frac{2\pi d\sin\theta}{\lambda}\,[0, 1, \ldots, M-1]^T. \tag{111}$$

Similarly, the rest elements of the Hessian matrix $\mathbf{H}$ can be calculated based on the first derivative of $\tilde{\mathbf{x}}$.

Appendix B
Derivation of the Cramer-Rao Bounds

Define all the unknown parameters as $\boldsymbol{\phi} = [\boldsymbol{\tau}, \boldsymbol{\xi}, \boldsymbol{\theta}, \overline{\boldsymbol{\beta}}, \breve{\boldsymbol{\beta}}] \in \mathbb{R}^{5U}$, where $\boldsymbol{\tau} = [\tau_1, \ldots, \tau_U]^T$, $\boldsymbol{\xi} = [\xi_1, \ldots, \xi_U]^T$, $\boldsymbol{\theta} = [\theta_1, \ldots, \theta_U]^T$, $\overline{\boldsymbol{\beta}} = [\mathrm{Re}\{\beta_1\}, \ldots, \mathrm{Re}\{\beta_U\}]^T$ and $\breve{\boldsymbol{\beta}} = [\mathrm{Im}\{\beta_1\}, \ldots, \mathrm{Im}\{\beta_U\}]^T$. Denote

$$\mathbf{b} = \mathrm{vec}(\mathbf{A}(\theta)\,\mathrm{diag}(\boldsymbol{\beta})\mathbf{X}(\boldsymbol{\tau}, \boldsymbol{\xi})) = \sum_{u=1}^{U}\beta_u\mathbf{x}(\tau_u, \xi_u)\otimes\mathbf{a}(\theta_u), \tag{112}$$

i.e., the signal part in (12), where

$$\mathbf{x}(\tau_u, \xi_u) = \begin{bmatrix} \mathbf{s}(\tau_u) \\ \mathbf{s}(\tau_u)^* \end{bmatrix}\odot\breve{\mathbf{d}}(\xi_u). \tag{113}$$

Given that $\mathbf{z}$ is white Gaussian noise, the expression of the FIM can be written as

$$\mathbf{F} = \frac{2}{\sigma^2}\,\mathrm{Re}\left\{\frac{\partial\mathbf{b}^H}{\partial\boldsymbol{\phi}}\frac{\partial\mathbf{b}}{\partial\boldsymbol{\phi}}\right\}, \tag{114}$$

where $\frac{\partial \mathbf{b}}{\partial \boldsymbol{\phi}} = \left[\frac{\partial \mathbf{b}}{\partial \boldsymbol{\tau}}, \frac{\partial \mathbf{b}}{\partial \boldsymbol{\xi}}, \frac{\partial \mathbf{b}}{\partial \boldsymbol{\theta}}, \frac{\partial \mathbf{b}}{\partial \overline{\boldsymbol{\beta}}}, \frac{\partial \mathbf{b}}{\partial \breve{\boldsymbol{\beta}}}\right] \in \mathbb{C}^{2LM \times 5U}$.

For $\frac{\partial \mathbf{b}}{\partial \boldsymbol{\tau}} = \left[\frac{\partial \mathbf{b}}{\partial \tau_1}, \ldots, \frac{\partial \mathbf{b}}{\partial \tau_U}\right]$, we have

$$\frac{\partial \mathbf{b}}{\partial \tau_u} = \beta_u \frac{\partial \mathbf{x}(\tau_u, \xi_u)}{\partial \tau_u} \otimes \mathbf{a}(\theta_u) = \beta_u \left\{ \begin{bmatrix} \frac{\partial \mathbf{s}(\tau_u)}{\partial \tau} \\ \frac{\partial \mathbf{s}(\tau_u)^*}{\partial \tau} \end{bmatrix} \odot \breve{\mathbf{d}}(\xi) \right\} \otimes \mathbf{a}(\theta_u). \tag{115}$$

For $\frac{\partial \mathbf{b}}{\partial \boldsymbol{\xi}} = \left[\frac{\partial \mathbf{b}}{\partial \xi_1}, \ldots, \frac{\partial \mathbf{b}}{\partial \xi_U}\right]$, we have

$$\frac{\partial \mathbf{b}}{\partial \xi_u} = \left[\beta_u \begin{bmatrix} \mathbf{s}(\tau_u) \\ \mathbf{s}(\tau_u)^* \end{bmatrix} \odot \frac{\partial \breve{\mathbf{d}}(\xi_u)}{\partial \xi_u}\right] \otimes \mathbf{a}(\theta_u), \tag{116}$$

For $\frac{\partial \mathbf{b}}{\partial \boldsymbol{\theta}} = \left[\frac{\partial \mathbf{b}}{\partial \theta_1}, \ldots, \frac{\partial \mathbf{b}}{\partial \theta_U}\right]$, we have

$$\frac{\partial \mathbf{b}}{\partial \theta_u} = \left[\beta_u \begin{bmatrix} \mathbf{s}(\tau_u) \\ \mathbf{s}(\tau_u)^* \end{bmatrix} \odot \breve{\mathbf{d}}(\xi_u)\right] \otimes \frac{\partial \mathbf{a}(\theta_u)}{\partial \theta_u}, \tag{117}$$

As to $\frac{\partial \mathbf{b}}{\partial \overline{\boldsymbol{\beta}}} = \left[\frac{\partial \mathbf{b}}{\partial \overline{\beta}_1}, \ldots, \frac{\partial \mathbf{b}}{\partial \overline{\beta}_u}\right]$, we have

$$\frac{\partial \mathbf{b}}{\partial \overline{\beta}_u} = \left[\begin{bmatrix} \mathbf{s}(\tau_u) \\ \mathbf{s}(\tau_u)^* \end{bmatrix} \odot \breve{\mathbf{d}}(\xi_u)\right] \otimes \mathbf{a}(\theta_u). \tag{118}$$

Similarly, $\frac{\partial \mathbf{b}}{\partial \breve{\boldsymbol{\beta}}} = \sqrt{-1}\frac{\partial \mathbf{b}}{\partial \breve{\boldsymbol{\beta}}}$. Based on the above derivations, we insert $\frac{\partial \mathbf{b}}{\partial \boldsymbol{\phi}}$ into (114). The CRBs of $\{\tau_u, \xi_u, \theta_u\}$ are given by

$$\mathrm{CRB}(\tau_u) = [\mathbf{F}^{-1}]_{u,u}, \tag{119}$$

$$\mathrm{CRB}(\xi_u) = [\mathbf{F}^{-1}]_{U+u,U+u}, \tag{120}$$

and

$$\mathrm{CRB}(\theta_u) = [\mathbf{F}^{-1}]_{2U+u,2U+u}. \tag{121}$$

Acknowledgment

The authors would like to thank Mr. Yifei Zhang for his help in the MDL-related simulation.

References

[1] P. Bello, "Joint estimation of delay, doppler, and doppler rate," *IRE Trans. Inf. Theory*, vol. 6, no. 3, pp. 330–341, 1960.

[2] R. Schmidt, "Multiple emitter location and signal parameter estimation," *IEEE Trans. Antennas Propag.*, vol. AP-34, no. 3, pp. 276–280, Mar. 1986.

[3] P. Zhang, J. Lu, Y. Wang, and Q. Wang, "Cooperative localization in 5G networks: A survey," *ICT Exp.*, vol. 3, no. 1, pp. 27–32, 2017.

[4] C. Laoudias, A. Moreira, S. Kim, S. Lee, L. Wirola, and C. Fischione, "A survey of enabling technologies for network localization, tracking, and navigation," *IEEE Commun. Surv. Tut.*, vol. 20, no. 4, pp. 3607–3644, Oct.–Dec. 2018.

[5] S. Kuutti, S. Fallah, K. Katsaros, M. Dianati, F. Mccullough, and A. Mouzakitis, "A survey of the state-of-the-art localization techniques and their potentials for autonomous vehicle applications," *IEEE Internet Things J.*, vol. 5, no. 2, pp. 829–846, Apr. 2018.

[6] A. Fascista, G. Ciccarese, A. Coluccia, and G. Ricci, "A localization algorithm based on V2I communications and AOA estimation," *IEEE Signal Process. Lett.*, vol. 24, no. 1, pp. 126–130, Jan. 2017.

[7] S. Sun, A. P. Petropulu, and H. V. Poor, "MIMO radar for advanced driver-assistance systems and autonomous driving: Advantages and challenges," *IEEE Signal Process. Mag.*, vol. 37, no. 4, pp. 98–117, Jul. 2020.

[8] L. Zhang and H. Wang, "Device-free tracking via joint velocity and AOA estimation with commodity WiFi," *IEEE Sensors J.*, vol. 19, no. 22, pp. 10662–10673, Nov. 2019.

[9] C. Knapp and G. Carter, "The generalized correlation method for estimation of time delay," *IEEE Trans. Acoust., Speech, Signal Process.*, vol. ASSP-24, no. 4, pp. 320–327, Aug. 1976.

[10] F. Viola and W. F. Walker, "Computationally efficient spline-based time delay estimation," *IEEE Trans. Ultrason., Ferroelectr., Freq. Control*, vol. 55, no. 9, pp. 2084–2091, Sep. 2008.

[11] R. Fleming, C. Kushner, G. Roberts, and U. Nandiwada, "Rapid acquisition for ultra-wideband localizers," in *Proc. IEEE Conf. Ultra Wideband Syst. Technol.*, 2002, pp. 245–249.

[12] J. Y. Lee and R. A. Scholtz, "Ranging in a dense multipath environment using an UWB radio link," *IEEE J. Sel. Areas Commun.*, vol. 20, no. 9, pp. 1677–1683, Dec. 2002.

[13] M. C. Vanderveen, B. C. Ng, C. B. Papadias, and A. Paulraj, "Joint angle and delay estimation (JADE) for signals in multipath environments," in *Proc. Conf. Rec. 30th Asilomar Conf. Signals, Syst. Comput.*, 1996, vol. 2, pp. 1250–1254 .

[14] C. S. See and A. Nehorai, "Estimating directions and times of arrival of multipath signals using a calibrated space-time antenna array," in *Proc. 9th IEEE Signal Process. Workshop Stat. Signal Array Process.*, 1998, pp. 364–367.

[15] Y. Wang, J. Chen, and W. Fang, "Joint estimation of DOA and delay using TST-MUSIC in a wireless channel," *IEEE Signal Process. Lett.*, vol. 8, no. 2, pp. 58–60, Feb. 2001.

[16] L. Liu and H. Liu, "Joint estimation of DOA and TDOA of multiple reflections in mobile communications," *IEEE Access*, vol. 4, pp. 3815–3823, 2016.

[17] A. van der Veen, M. C. Vanderveen, and A. J. Paulraj, "Joint angle and delay estimation using shift-invariance properties," *IEEE Signal Process. Lett.*, vol. 4, no. 5, pp. 142–145, May 1997.

[18] A. Richter, D. Hampicke, G. Sommerkorn, and R. S. Thoma, "Joint estimation of DOD, time-delay, and DOA for high-resolution channel sounding," in *Proc. IEEE 51st Veh. Technol. Conf. Proc.*, 2000, vol. 2, pp. 1045–1049 .

[19] H. Wang and J. Wang, "Joint two dimensional DOA and multipath time delay estimation in rectangular planar array," in *Proc. IEEE Region 10 Conf.*, 2007, pp. 1–4.

[20] A. L. Swindlehurst, "Time delay and spatial signature estimation using known asynchronous signals," *IEEE Trans. Signal Process.*, vol. 46, no. 2, pp. 449–462, Feb. 1998.

[21] A. Bazzi, D. T. M. Slock, and L. Meilhac, "Efficient maximum likelihood joint estimation of angles and times of arrival of multiple paths," in *Proc. IEEE Globecom Workshops*, 2015, pp. 1–7.

[22] F. Bellili, S. B. Amor, S. Affes, and A. Ghrayeb, "Maximum likelihood joint angle and delay estimation from multipath and multicarrier transmissions with application to indoor localization over IEEE 802.11ac radio," *IEEE Trans. Mobile Comput.*, vol. 18, no. 5, pp. 1116–1132, May 2019.

[23] M. Wax and A. Leshem, "Joint estimation of time delays and directions of arrival of multiple reflections of a known signal," in *Proc. IEEE Int. Conf. Acoust., Speech, Signal Process. Conf. Proc.*, 1996, vol. 5, pp. 2622–2625.

[24] B. H. Fleury, M. Tschudin, R. Heddergott, D. Dahlhaus, and K. Ingeman Pedersen, "Channel parameter estimation in mobile radio environments using the SAGE algorithm," *IEEE J. Sel. Areas Commun.*, vol. 17, no. 3, pp. 434–450, Mar. 1999.

[25] F. Antreich, J. A. Nossek, and W. Utschick, "Maximum likelihood delay estimation in a navigation receiver for aeronautical applications," *Aerosp. Sci. Technol.*, vol. 12, no. 3, pp. 256–267, 2008.

[26] F. Antreich, J. A. Nossek, G. Seco-Granados, and A. L. Swindlehurst, "The extended invariance principle for signal parameter estimation in an unknown spatial field," *IEEE Trans. Signal Process.*, vol. 59, no. 7, pp. 3213–3225, Jul. 2011.

[27] Y.-Y. Dong, C.-X. Dong, W. Liu, and M.-M. Liu, "DOA estimation with known waveforms in the presence of unknown time delays and doppler shifts," *Signal Process.*, vol. 166, pp. 107232.1–107232.7, 2020, Art. no. 107232.

[28] Y. Jiang, B. Daneshrad, and G. J. Pottie, "A practical approach to joint timing, frequency synchronization and channel estimation for concurrent transmissions in a MANET," *IEEE Trans. Wireless Commun.*, vol. 16, no. 6, pp. 3461–3475, Jun. 2017.

[29] I. Ziskind and M. Wax, "Maximum likelihood localization of multiple sources by alternating projection," *IEEE Trans. Acoust., Speech, Signal Process.*, vol. 36, no. 10, pp. 1553–1560, Oct. 1988.
[30] H. Akaike, *Information Theory and an Extension of the Maximum Likelihood Principle*. New York, NY, USA: Springer, 1998.
[31] "Modeling by shortest data description," *Automatica*, vol. 14, no. 5, pp. 465–471, 1978.
[32] M. Wax and T. Kailath, "Detection of signals by information theoretic criteria," *IEEE Trans. Acoust., Speech, Signal Process.*, vol. ASSP-33, no. 2, pp. 387–392, Apr. 1985.
[33] D. Chu, "Polyphase codes with good periodic correlation properties (corresp.)," *IEEE Trans. Inf. Theory*, vol. IT-18, no. 4, pp. 531–532, Jul. 1972.
[34] S. Boyd and L. Vandenberghe, *Convex Optimization*. Cambridge, U.K.: Cambridge University Press, 2004.
[35] X. Wei, Y. Jiang, Q. Liu, and X. Wang, "Calibration of phase shifter network for hybrid beamforming in mmwave massive MIMO systems," *IEEE Trans. Signal Process.*, vol. 68, pp. 2302–2315, 2020.
[36] C. D. Meyer, *Matrix Analysis and Applied Linear Algebra*. SIAM, 2000.

Zhiyu Yang (Student Member, IEEE) received the B.S. degree in communication engineering from Fudan University, Shanghai, China, in 2019. He is currently working toward the M.E. degree in communication and information systems with Fudan University, Shanghai, China. His research interests include signal processing for wireless communication, channel estimation and localization.

Rui Wang (Student Member, IEEE) received the B.S. degree in communication engineering from Northeastern University, Shenyang, China, in 2018. She is currently working toward the Ph.D. degree with the Department of Communication Science and Engineering, Fudan University, Shanghai, China,. Her research interests include MIMO wireless communication, relay network, and signal processing for wireless communication.

Yi Jiang (Member, IEEE) received the B.S. degree in electrical engineering and information science from the University of Science and Technology of China (USTC), Hefei, China, in 2001, and the M.S. and Ph.D. degrees in electrical engineering from the University of Florida, Gainesville, FL, USA, in 2003 and 2005, respectively. In 2005, he was a Research Consultant with Information Science Technologies Inc., Fort Collins, CO, USA. From 2005 to 2007, he was a Postdoctoral Researcher with the University of Colorado, Boulder, CO, USA. He moved to San Diego, CA, USA, in 2007, and worked for multiple companies, including NextWave Wireless from May 2007 to July 2008, Qualcomm Corporate Research and Development from August 2008 to May 2012, IAA Incorporated from June 2012 to January 2013, and Silvus Technologies from February 2013 to July 2016. He also worked as an Adjunct Researcher with the Electrical Engineering Department, University of California at Los Angeles, Los Angeles, CA, USA, from October 2014 to July 2016. He joined Fudan University in August 2016, and is currently a Professor of the Department of Communication Science and Engineering, Fudan University, China. His research interests include array signal processing and mobile ad hoc networks. He is the Editor of IEEE WIRELESS COMMUNICATIONS LETTERS.

Jian Li (Fellow, IEEE) received the M.Sc. and Ph.D. degrees in electrical engineering from The Ohio State University, Columbus, OH, USA, in 1987 and 1991, respectively. She is currently a Professor with the Department of Electrical and Computer Engineering, University of Florida, Gainesville. Her current research interests include spectral estimation, statistical and array signal processing, and their applications to radar, sonar, and biomedical engineering. Dr. Li's publications include *Robust Adaptive Beamforming* (2005, Wiley), *Spectral Analysis: the Missing Data Case* (2005, Morgan and Claypool), *MIMO Radar Signal Processing* (2009, Wiley), and *Waveform Design for Active Sensing Systems - A Computational Approach* (2011, Cambridge University Press). Dr. Li is a Fellow of IET. She is also a Fellow of the European Academy of Sciences (Brussels). She was the recipient of the 1994 National Science Foundation Young Investigator Award and the 1996 Office of Naval Research Young Investigator Award. She was an Executive Committee Member of the 2002 International Conference on Acoustics, Speech, and Signal Processing, Orlando, Florida, May 2002. She was an Associate Editor for the IEEE TRANSACTIONS ON SIGNAL PROCESSING from 1999 to 2005, an Associate Editor for the *IEEE Signal Processing Magazine* from 2003 to 2005, and a member of the Editorial Board of *Signal Processing*, a publication of the *European Association for Signal Processing (EURASIP)*, from 2005 to 2007. She was a member of the Editorial Board of the *IEEE Signal Processing Magazine* from 2010 to 2012. She is currently a member of the Sensor Array and Multichannel Technical Committee of the IEEE Signal Processing Society. She is a coauthor of the paper that has received the M. Barry Carlton Award for the Best Paper published in IEEE TRANSACTIONS ON AEROSPACE AND ELECTRONIC SYSTEMS in 2005. She is also a coauthor of a paper published in IEEE TRANSACTIONS ON SIGNAL PROCESSING that has received the Best Paper Award in 2013 from the IEEE Signal Processing Society